



UNIVERSIDAD NACIONAL DE COLOMBIA

Diseño y Construcción de un banco de pruebas con iluminación multiespectral para el estudio del estado de maduración en aguacates.

Víctor Alejandro Patiño Martínez

Universidad Nacional de Colombia
Facultad de Ingeniería y Arquitectura
Departamento de Ingeniería Eléctrica y Electrónica y computación
Manizales, Colombia
2023

Diseño y Construcción de un banco de pruebas con iluminación multispectral para el estudio del estado de maduración en aguacates.

Víctor Alejandro Patiño Martínez

Tesis presentada como requisito parcial para optar al título de:
Magister en Ingeniería - Automatización Industrial

Director:

Ph.D. Juan Bernardo Gómez Mendoza

Codirector:

Ph.D. Gustavo Adolfo Osorio Londoño

Línea de Investigación:

Diseño de producto electrónico

Grupo de Investigación:

Percepción y Control Inteligente - PCI

Universidad Nacional de Colombia
Facultad de Ingeniería y Arquitectura
Departamento de Ingeniería Eléctrica y Electrónica y computación
Manizales, Colombia
2023

A mis padres, mi hermana y mi novia

Agradecimientos

Agradezco a mi familia por el apoyo que me brindaron durante toda mi formación académica, a mi novia Sharon quien con su amor y paciencia me alentó a enfrentar cada obstáculo del proceso. A mis directores de tesis Juan Bernardo y Gustavo Osorio quienes con su conocimiento me guiaron y me ayudaron a cumplir las expectativas generadas al entrar en este proceso de formación. A la Universidad Nacional de Colombia sede Manizales por la beca concedida para poder llevar a cabo esta maestría. De igual modo a todas las personas que de alguna manera contribuyeron con el diseño del sistema multiespectral.

Resumen

Diseño y Construcción de un banco de pruebas con iluminación multiespectral para el estudio del estado de maduración en aguacates.

La exportación de aguacates en Colombia ha aumentado en los últimos años. Una de las etapas clave del proceso de producción es conocer el grado de madurez del aguacate que se va a cosechar. Existe una correlación entre la materia seca de un aguacate y su estado de maduración. Sin embargo, la estimación de la materia seca por medios físicos es un proceso que consume mucho tiempo y conlleva grandes pérdidas. Existen varios estudios sobre la relación entre imágenes multiespectrales de aguacates y su materia seca. Esta tesis presenta los detalles sobre el diseño y la construcción de un sistema de imágenes multiespectrales basado en Leds. El diseño se dividió en tres partes principales: mecánica, hardware electrónico y firmware. Una vez probado el sistema, se tomaron imágenes de 14 aguacates para obtener una primera aproximación a la estimación de la materia seca, utilizando técnicas de uso común en reconocimiento de patrones como LDA, distancia de Mahalanobis y mapas auto-organizativos. Nuestros mejores resultados se obtuvieron utilizando la distancia de Mahalanobis, que da un error relativo máximo del 14,77 %.

Palabras clave: Sistema de imágenes multiespectrales basado en leds, Materia seca del aguacate, Hardware Electronico, Mecánica, Firmware, Algoritmos de clasificación, LDA, S.O.M, Distancias de Mahalanobis.

Abstract

Design and construction of a multispectral illumination test bench for the study of the ripening stage of avocados.

The exportation of avocados in Colombia has increased in the last few years. One of the key stages of the production process is to know the ripeness level of the avocado that is going to be harvested. There is a correlation between the dry matter of an avocado and its ripeness state. Nevertheless, dry matter estimation by physical means is a time-consuming and wasteful process. There are several studies on the relationship between multispectral images of avocados and their dry matter. This thesis presents the details on the design and construction of a LED-Based Multispectral Imaging System. The design was divided into three main parts: mechanical, electronic hardware, and firmware. Once the system was proof tested, images were taken from 14 avocados in order to obtain a first approximation to the estimation of the dry matter, using techniques that are commonly used in pattern recognition such as LDA, Mahalanobis distance, and Self-organizing-maps. Our best results were

achieved using the Mahalanobis distance, which gives a maximum relative error of 14.77% .

Keywords: LED-Based Multispectral Imaging System, Avocado dry matter, Hardware, Mechanical, Firmware, Classification algorithms, LDA, S.O.M, Mahalanobis distances

Content

Agradecimientos	VII
Resumen	IX
Lista de figuras	XIII
Lista de tablas	1
1. Introducción	2
2. Mechanical and Electronic Design	6
2.1. Mechanical Design	7
2.1.1. Shape of the enclosure	8
2.1.2. Quantity of light sources	8
2.1.3. Camera to be used	9
2.1.4. Size of the enclosure	10
2.1.5. Material to be used in the enclosure	10
2.2. Electronic hardware design	12
2.2.1. Research stage	14
2.2.2. Implementation	17
3. System integration and firmware design	20
3.1. System Integration	20
3.1.1. Electrical connections	22
3.1.2. Camera trigger	22
3.1.3. User to master board communication	23
3.1.4. Master to slave board communication	23
3.2. Firmware architecture	23
3.2.1. Identification stage	24
3.2.2. Execution stage	25
3.2.3. Multiple ON-OFF wavelength times command	29
3.3. Light source calibration values	30
4. Multispectral image acquisition and dry matter extraction	31
4.1. Image acquisition	31

4.2. Dry matter in avocado	33
4.2.1. Dry matter extraction method	33
4.3. Exercise with avocado dry matter	35
4.3.1. Masking of the avocados in the images	36
4.3.2. Reflectance normalization	37
5. Avocado dry matter results	41
5.1. Visualization of the Spectral avocado information using PCA	42
5.1.1. LDA classification and dry matter approximation	42
5.1.2. Pixel-wise classification using the Mahalanobis distance	49
5.1.3. Self-Organizing maps classification	51
6. Conclusions and future work	54
6.1. Conclusions	54
6.2. Future work	55
A. Anexo: Total variation in specular light	56
A.0.1. Tools	56
A.0.2. Setup	56
A.0.3. Total variation	57
A.0.4. Total intensity	58
A.0.5. Equation approximation using algorithms	58
A.0.6. Optimization	60
Bibliografía	62

List of Figures

1-1. Multispectral system schematic.	3
1-2. Hierarchical schematic of the electronic board.	4
2-1. 3D representation of the multispectral acquisition system.	7
2-2. Structure wall dimensions.	8
2-3. Light source distribution.	9
2-4. Flea3 Quantum Efficiency [Grey, 2022].	10
2-5. Camera support structure design.	11
2-6. Structure dimensions.	12
2-7. 3D part for angular movement of the light source.	13
2-8. First light source board prototype.	13
2-9. First Light source control board prototype.	14
2-10. First LED current control circuit.	15
2-11. Second LED current control circuit.	16
2-12. Double footprint LED implementation.	17
2-13. Reconfigurable LED current control using series resistor.	18
2-14. FL7760 recommended schematics [Onsemi, 2022].	19
2-15. Reconfigurable LED current control using the FL7760 driver.	19
2-16. External board connectors pinout.	19
3-1. Dome images	21
3-2. Dataflow block diagram.	22
3-3. Board diagram connection. Blue connectors were used for board communication.	23
3-4. Trigger control circuit.	24
3-5. Communication protocol diagram.	25
3-6. Firmware flow chart.	26
3-7. ID diagram distribution.	27
3-8. LED number distribution.	28
3-9. Camera port pinout [Grey, 2023].	30
4-1. Color checker images under different lighting.	32
4-2. Color checker RGB image.	33
4-3. Avocado images under different lighting.	34
4-4. Histograms of the first two avocados captured.	35

4-5. Avocado wavelength reflectance [Lyu, 2019].	36
4-6. Avocados capture	37
4-7. Avocado synthetic image.	38
4-8. Example mask used in avocado images.	40
4-9. Histograms of avocado synthetic image.	40
5-1. Avocado pixel information after PCA.	43
5-2. Avocados representation after PCA reduction.	44
5-3. PCA vs LDA differences [Avila, 2022].	45
5-4. Avocados representation after PCA reduction.	46
5-5. Confusion matrix computed using the reference data.	47
5-6. Confusion matrix computed using remaining avocados.	47
5-7. Self-organized maps with 7 avocados and 7 points	52
A-1. Total variation in specular light HLBD.	57
A-2. LEDs bar.	57
A-3. Control board.	58
A-4. Setup	58
A-5. Captured heat maps.	59
A-6. Obtained graphs.	61
A-7. Equation graphs obtained.	61
A-8. Cost function graph.	61

List of Tables

4-1. Avocado experiments record.	39
5-1. Avocado classification LDA with statistic mode.	48
5-2. Avocado classification LDA with statistic median.	48
5-3. LDA Avocado classification with probabilities and statistic median.	49
5-4. Avocado classification with minimum Mahalanobis distance	50
5-5. Avocado classification with two minimum Mahalanobis distance	51
5-6. Avocado classification with two consecutive minimum Mahalanobis distance.	51
5-7. Self-organized points gotten values by mean.	52
5-8. Avocado classification with 7 avocados using self-organized maps.	53
A-1. Total variation vs angle.	60
A-2. Total intensity vs angle.	60

1. Introducción

The avocado is an important exportation product in Colombia, whose demand is expected to increase [Peinado et al., 2020]. One of the most critical parts in the food chain of the avocado is to know when it should be harvested from the tree. In the literature, there are studies about the relation between an avocado's ripeness state and its dry matter content; for instance, [Lee et al., 1983] shows how the ripeness state of the avocado can be validated based on its dry matter. Based in [Carvalho et al., 2015], in Colombia, the minimum amount of dry matter for an avocado to be harvested has been established at 24%.

Dry matter measurement is done by an invasive, wasteful, and time-consuming process [Ordoñez, 2019]. There are articles in which multispectral light has been used to approximate an avocado's dry matter value with a non-invasive process. For example, in ([Lyu, 2019]), the author explores how neural network methods can approximate the dry matter using multispectral images of avocados; in the analysis, the authors measures the reflectance of the avocado in the range between 400 nm to 1000nm.

The available multispectral devices are expensive due to their technology. This work aims to present the design and construction of a narrow-band high-power LED based multispectral system, aimed towards the exploration of the spectral properties of agricultural produces. The approach presented in this work comprises three different parts in the design: a mechanical design of the enclosure and mountings, the hardware design of the electronic boards that carry the lights and the control logic, and the firmware design.

In Fig 1-1, a schematic diagram of the physical deployment of the proposed solution is presented. The diagram shows the main elements of the design with the exception of the firmware.

Multispectral captures can be highly affected by external lights. In order to limit the amount of ambient light getting into the scene, an enclosure for the system was designed with the help of the Dynamics maker team (a company in charge of creating mechanical parts), looking for a solution to the geometrical constraints imposed by the application.

Two of the main types of light that form an image are specular and diffused light [Matusik, 2003]. Diffused light gives relevant information about the captured objects in the image; on the other side, the specular light generates bright spots in the object that saturate some pixels of the sensor. Based on [Jain et al., 1995] can be inferred that the specular light is related to the angle between the light source and the sensor camera; The maximum specular light is present when the angle between the camera and the light source is 0 grades, its minimum effect can be seen when they are perpendicular. More information

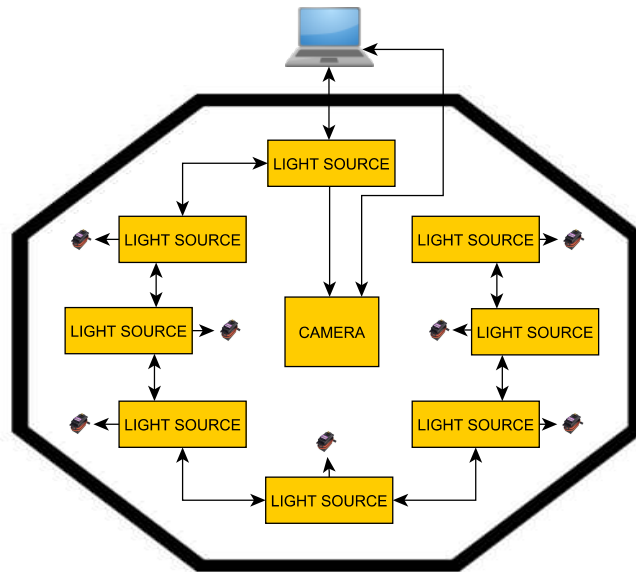


Figure 1-1.: Multispectral system schematic.

about specular light will be found in the appendix A.

Shadows are generated by the absence of light in parts of an object; they can be produced due to concave shapes. This problem can be solved by increasing the number of light sources, and distributing them to cover the self-occluded parts of the objects.

The electronic hardware design aims to solve two main problems: the need to control the LEDs' brightness, and the implementation of the circuitry that allows the communication between boards. For controlling the LED brightness, an IC controller was used; it was able to modify the LED's intensity based on the LED's nominal current. The controller uses a PWM signal generated by an MCU as reference. The board designed supports up to 8 different wavelengths, with a total of three LEDs per wavelength in serial connection. In some parts of the document, I refer to this boards to as light sources.

The boards communicate between them using a UART interface. It was chosen due to its easy hardware and firmware design and implementation. Two connectors were placed into the hardware design to bridge the board to two more boards in a cascade configuration. Apart from the UART interface, four GPIO lines were added for high-speed synchronization between the boards. Fig 1-2 depicts the hardware design of the light source board. Part of the hardware design was based on existing designs that are available in the market, such as the Keyence systems [KEYENCE, 2023], as well as a form of evolution of the work in [Tamayo Monsalve, 2020].

In the firmware design, three main functions were identified. The first was the need for a PWM signal generation for the IC LED controllers; the second was the need for a commu-

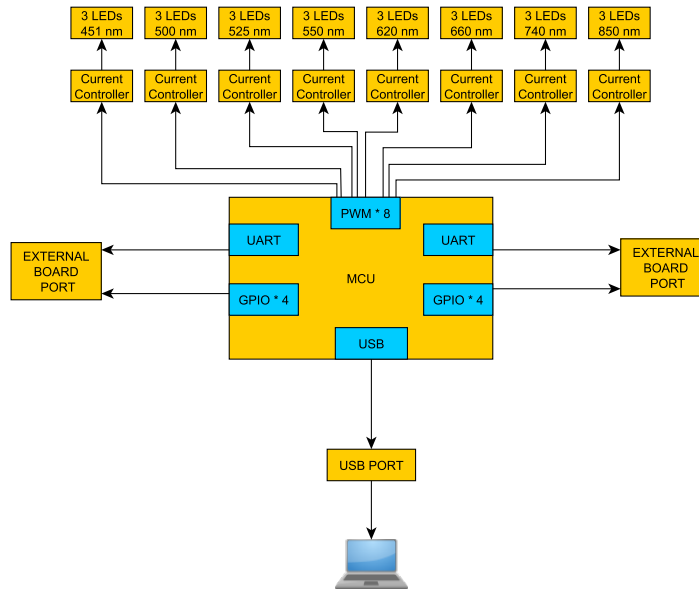


Figure 1-2.: Hierarchical schematic of the electronic board.

nication stack between boards and users; and the third was the synchronization and control of the camera trigger for acquisition.

The main contributions of this Thesis are related to the design and construction of a cost-effective multispectral imaging system based on narrow-band high-power LEDs. The mechanical design isolates the image acquisition process from the influence of external lights, while minimizing the effects of other phenomena like specular and diffuse light, by providing the ability to control the light source's incident angle. On the other hand, the multispectral light control was carefully designed to meet the requirements regarding the nominal current for the power LEDs and the brightness control using a PWM signal. Regarding firmware development, a robust communication protocol was proposed and implemented based on a cascade connection, intended to be used with up to eight boards (although it may work with more). Finally, the system was used to obtain a first approximation to establishing a relationship between avocado dry matter and its multispectral images, getting a maximum relative error of 14.77% using the Mahalanobis distance.

The structure of this document is as follows:

The second chapter depicts the insights of the mechanical design of the enclosure, presenting the main decisions regarding the structure; as well as the design of the printed electronic board that carries the LEDs, and the analysis of the implemented circuitry solutions.

The third chapter describes the development of the main algorithms in the firmware. The solution is presented by using written descriptions and block diagrams that explain how the light source boards work. The integration of the system is also discussed in this chapter,

including how the electrical connections were made.

The fourth chapter shows the results obtained in the tests carried out to validate the correct function of the system, and the process done for capturing a group of images of avocados, and measuring their dry matter by following the standard process stated in literature.

The fifth chapter presents the algorithms implemented to find a relationship between the dry matter and the multispectral information of the images of the avocados. Different methods like LDA, Mahalanobis distance, and Self-organizing maps are used in this chapter, and the relative error of the before methods were calculated to validate their accuracy.

The sixth chapter draws the conclusions of this work, and some recommendations for future work.

2. Mechanical and Electronic Design

One of the main factors that can affect a multispectral system is the influence of external light (sunlight, lamps). To achieve a consistent behavior and to avoid intensity changes due to disturbances like the weather or location was essential to reduce the variables affecting the system. Works like [Tamayo Monsalve, 2020] or [Lyu, 2019] have removed the external light by using an enclosure; in this thesis, a similar solution was designed.

With the implementation of an enclosure, a challenge is to minimize the reflections inside the structure in order to avoid unwanted light readings. The shape of the enclosure affects the number of reflections, so a cylindrical shape was the first possible solution because it creates a surrounding effect. However, a cylindrical shape is hard to construct and difficult with most industrial materials. Therefore, the design led to an octagonal shape trying to get close to a cylinder. The material selected for the structure was MDF due to its thickness and malleability. Additionally, the walls were covered with black 3.0 paint to reduce the reflection of light inside the structure.

The structure was designed to capture products with a maximum size of 15.8 * 11.9 cm, which is more than the maximum size needed for capturing avocados ([REY, 2022]). The final dimensions for the structure were 1.36 x 1.36 x 0.5 meters: On Fig2-1, there is a 3D representation of the enclosure with the representation of an avocado to give a visual idea on the dimensions.

There are two main types of light phenomena that form an image. The first one is the diffuse reflection light, which will give the relevant information, and the second one is the specular light, which generates bright spots ([Matusik, 2003]). Based on [Jain et al., 1995], there is a relation between the specular light and the angle formed between the light source, the object, and the camera. An experimental study was done on this topic and can be found in appendix A. Servos were added to the structure to be able to move the light source's angle and find a suitable setup during the capture process. In addition, shadows are also a problem in image capturing. They are created due to the concave shape of the avocados and the light source's position. The shadows can be decreased by adding more light sources to illuminate the scene; therefore the system was designed to have up to 8 light sources with 45 degrees angle between them. If not needed, a few number of light sources can be installed.

A key feature in a LED-based multispectral imaging system is the ability to control the amount of light in the scene to avoid the saturation of the camera sensor. Hence, an IC driver controller was used for each of the 8 groups of LEDs used in the PCBs. According to the wavelength the driver controls the current and brightness of the three LEDs in serial

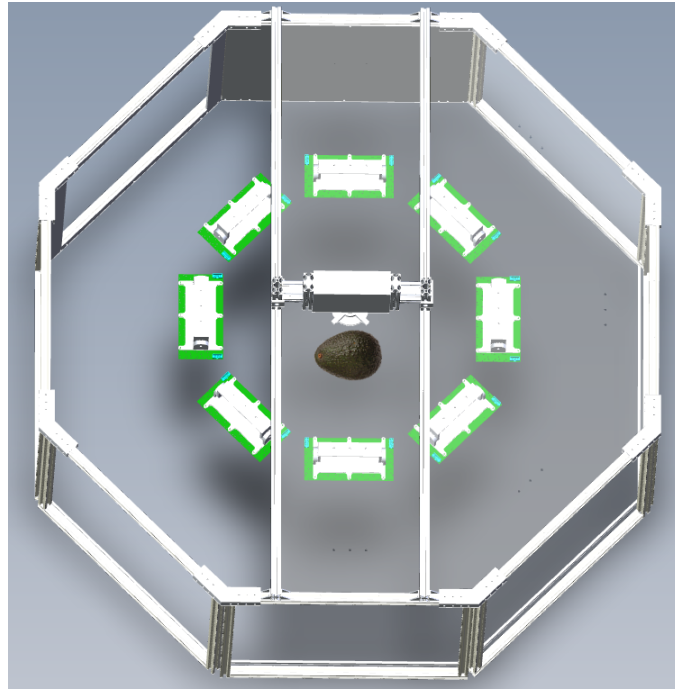


Figure 2-1.: 3D representation of the multispectral acquisition system.

connection; while providing a high power efficiency.

In the market, high-power LEDs do not follow a global footprint, so the three more common footprints were added to the PCB to be able to use different packages in the future.

As the system was designed to be conformed by multiple boards, a communication protocol was needed. For this purpose the USB, UART and four GPIO pins of the microcontroller were selected to handle the communications and synchronization between the User (PC) and the lighting boards.

2.1. Mechanical Design

In the mechanical design, multiple topics were discussed. Some of the main topics that directly affected the design of the enclosure were:

- Shape of the enclosure.
- Quantity of light sources.
- Camera to be used.
- Size of the enclosure.
- Material to be used in the enclosure.

- reflectance of the surface inside of the structure.

2.1.1. Shape of the enclosure

In image capturing is essential to provide a high uniformity of light without having bright spots. The cylindrical shape will provide a uniform distribution and reflection of light due to the way it reflects in the surfaces, on [Martin, 2009] is shown how a dome (sphere shape) can create an entire bright field. However, building a cylindrical shape is not accessible from a mechanical point of view because not all materials will allow this kind of shape. The solution found was to select an octagonal shape, not as good as a cylindrical shape, but with eight sides, the structure can resemble a cylindrical shape. A shape with a more significant number of sides will have better performance, but it increments the complexity of the design. In Fig 2-2, there is a picture provided by the dynamics maker team; they are a company that helped us with the mechanical design.

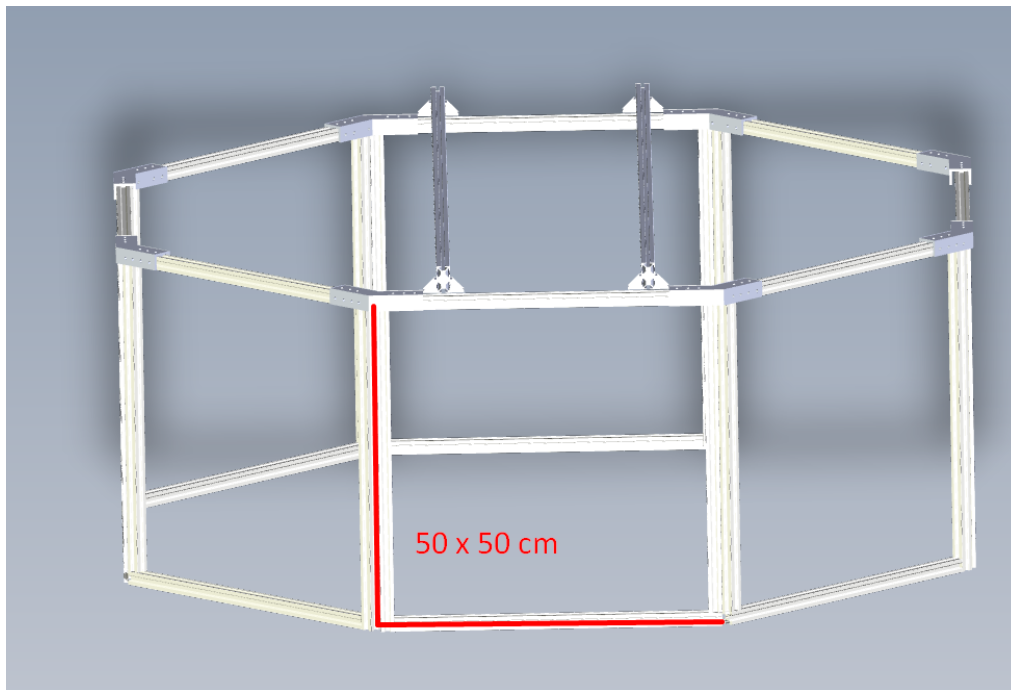


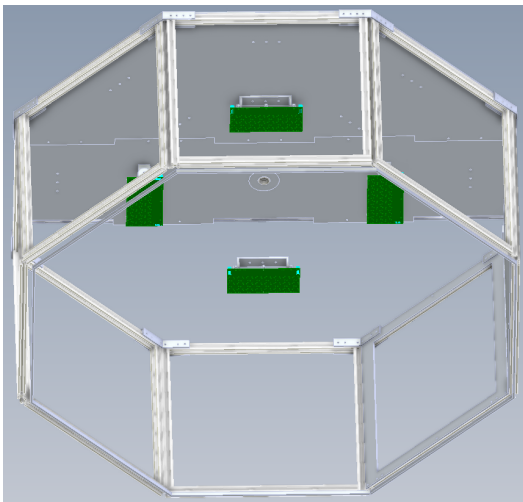
Figure 2-2.: Structure wall dimensions.

2.1.2. Quantity of light sources

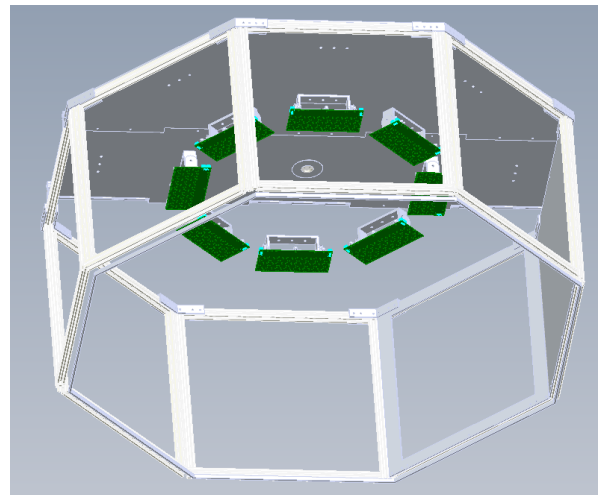
One of the main problems with multispectral system captures would be the generation of shadows into the captured images due to the concave shapes of the objects and the position of the light sources.

The selection of number of light boards was based on three points. The first one was the amount of light needed; the second one was the shadows in the object generated by the position of the light sources; and the third one was the specular and diffused light generated by the angle between the light sources and the camera.

The amount of light is not a problem since the capturing area is isolated by the mechanical structure which allow the system to work fine with few LEDs. This assumption was validated with three high-power LEDs in a controlled ambient. The second and third points depended directly on the position of the light source and the light direction angle. Therefore, after analyzing the complexity and cost of adding each light source, eight boards represent a good compromise. This number of light sources allows an angle of 45 degrees between them. The number of light sources can be decreased by half into the same structure if needed, with an angle of 90 degrees between them. Fig 2-3 represents the eight and four board configurations.



(a) Four light source.



(b) Eight light source.

Figure 2-3.: Light source distribution.

2.1.3. Camera to be used

The main camera used was Flea3 GigE; this was used before in the Thesis [Tamayo Monsalve, 2020], in which the author used it for the study of coffee cherries. The quantum efficiency of the camera sensor is shown in Fig 2-4, and more specs can be seen in [Grey, 2022].

The Flea3 GigE camera has an aspect ratio of 4:3 with a diagonal size of 0.25; the used lens has a focal distance of 16mm; with those values, the diagonal of the area to be captured was calculated with the equation EQ (2-1); where $\mathbf{ds}_{c,a}$ is the diagonal size of the captured area, $\mathbf{d}_{o,l}$ refers to the distance between the lens of the camera and the objective area, $\mathbf{ds}_{c,s}$ is the diagonal size of the camera sensor and \mathbf{f}_d represents the focal distance of the lens; with a $\mathbf{d}_{o,l}$

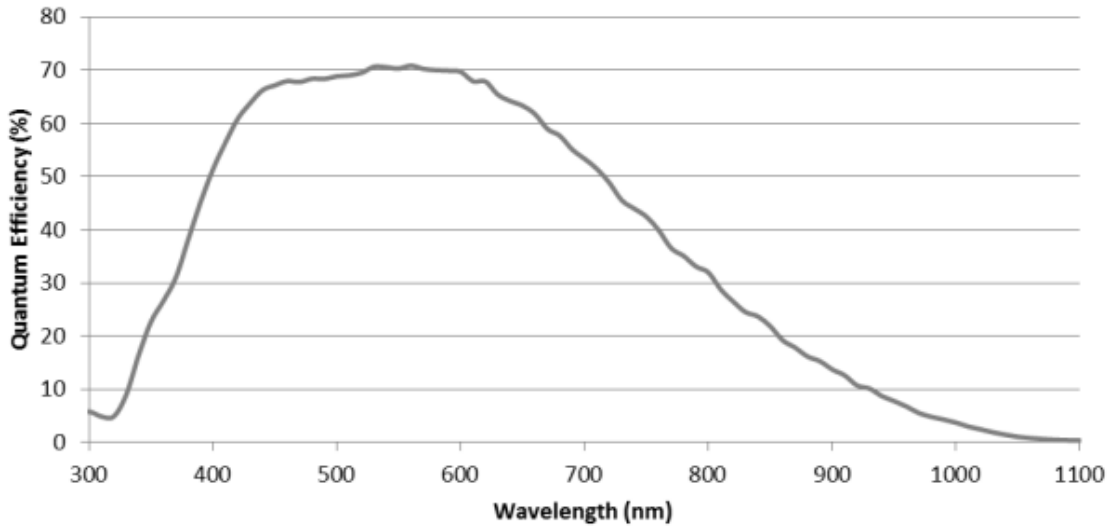


Figure 2-4.: Flea3 Quantum Efficiency [Grey, 2022].

of 50 cm, the total capture area is 15.8 x 11.9 cm.

$$ds_{c,a} = \frac{d_{o,l} * ds_{c,s}}{f_d} \quad (2-1)$$

In the future, the Canon EOS 90D camera will be used too. This camera has different dimensions than the Flea3 GigE. Therefore, the Dynamics Maker team created an additional part to handle both cameras. In Fig 2-5, the constructed structure for both cameras can be seen.

2.1.4. Size of the enclosure

The size of each side of the enclosure was defined as 50 x 50 cm; was selected based in that a height of 50 cm will be needed and a 50 x 50 cm will be a good area for building a door to interact with the internal parts of the enclosure. The total size of the enclosure was conditioned by the eight sides selected and their length. The total size obtained was 1.36 meters, as shown in Fig 2-6.

2.1.5. Material to be used in the enclosure

The material selection was based on three main topics:

- Material thickness
- Material malleability

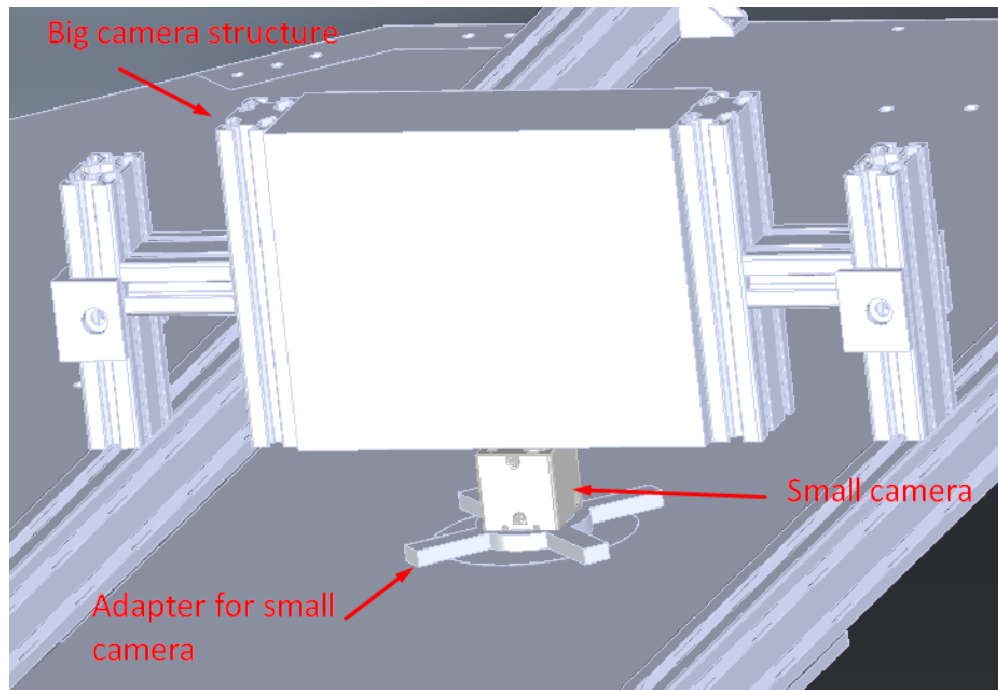


Figure 2-5.: Camera support structure design.

- Material reflectance

The material's thickness was necessary to be defined because it can affect the structure's robustness. A large wall with a small thickness will end in a weak structure. The malleability properties of the material influence the type of structures that can be constructed.

The Dynamics Maker team recommended the use of MDF material for the structure. This material is easy to cut and can be found in the market with different thicknesses; however, the problem with the material was its reflectance due to it does not have a high absorption. The multispectral system should only capture the light coming from the object and not from the surface; hence the absorption of the material has to be almost 100%. As a solution, two painting options were found in the market: vantablack and black 3.0. Vantablack is a painting used in [Adams et al., 2019]; it has a light absorption close to 99.965%; however, this paint was discarded because it was expensive and hard to find. The Black 3.0 option was the second option with a light absorption close to 99%; it has been used in other research like in [Liu et al., 2022]. Some of its specifications can be found in [CULTUREHUSTLE, 2023].

After defining the paint to be used, all the needed parts were designed by Dynamics Maker, and some of them were 3D printed. An example of a 3D part printed was the light source coupling piece; it was designed to change its angle, as can be seen in Fig 2-7.

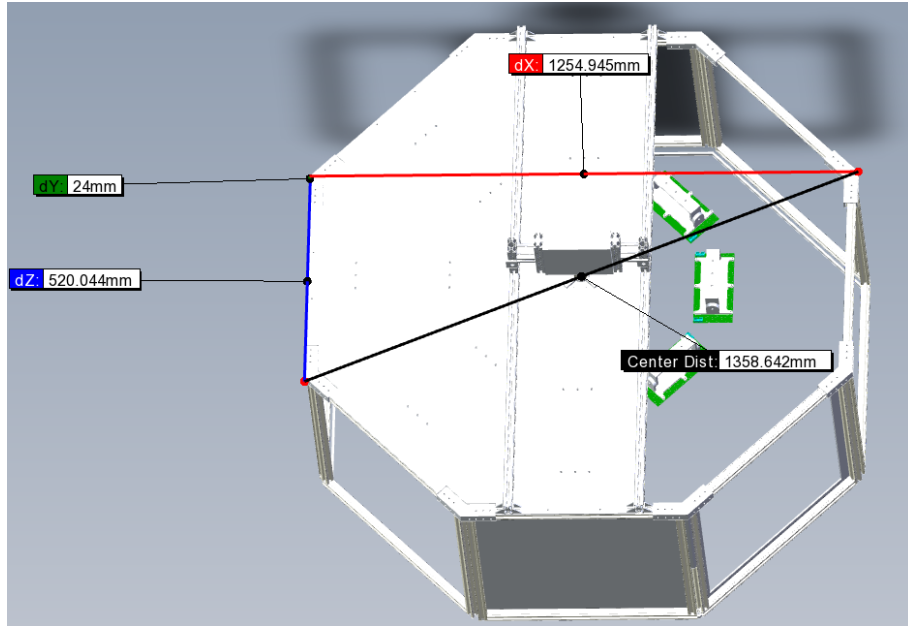


Figure 2-6.: Structure dimensions.

2.2. Electronic hardware design

The hardware design was done taking into account the first prototype done by the PCI and SHAC groups of the National University. This prototype had a total of 8 different groups of wavelenghts with 3 LEDs per group; the principal objective of the first prototype was to test different ways of controlling the nominal current of a LED. Fig 2-8 and Fig 2-9 are pictures of the PCI-SHAC group version. After testing this prototype, some improvements were found to be applied into a new version; those improvements were:

- The prototype had a mechanical design that was hard to handle inside a structure due to its shape.
- The prototype can only turn on 3 of the eight wavelenghts; hardware changes were needed to turn on other wavelenghts.
- For the principal MCU, a development board was used; it increased the system's cost and limited the hardware and mechanical design of the board.
- The system needed to be more easily scalable because there was no easy way to interconnect it with other boards.
- LEDs are fabricated with different footprints; the prototype was done for some specific footprints, which limits the possible wavelenghts to be used.

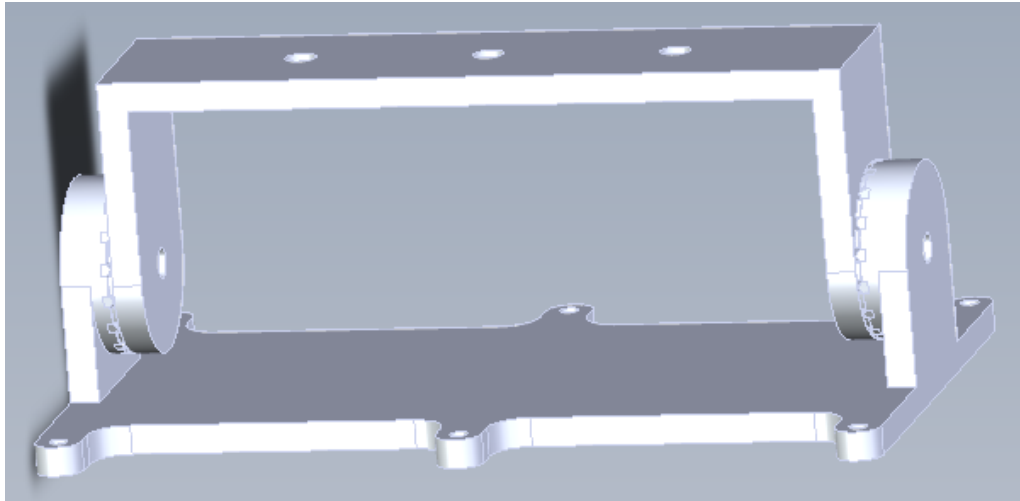


Figure 2-7.: 3D part for angular movement of the light source.

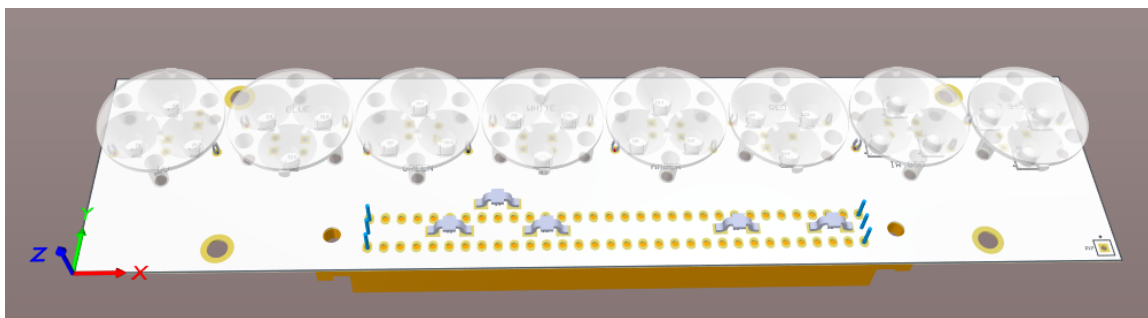


Figure 2-8.: First light source board prototype.

A list of requirements was defined based on works like [Kim et al., 2004], the before-detected improvements of the first prototype, and opinions from different team members related to the project. The requirements defined were:

- The light source board should be able to control eight different LED wavelengths simultaneously without hardware changes.
- The light source board should be able to change the nominal current of the LEDs.
- The light source board should be able to control the brightness of each LED wavelength independently.
- The light source board should be able to receive commands by USB.
- The light source board should have a mechanical design to be easily installed into a structure.

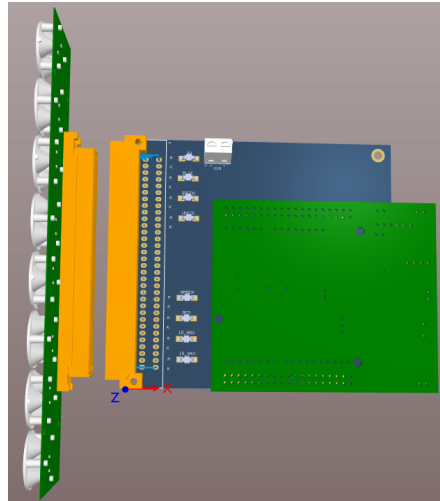


Figure 2-9.: First Light source control board prototype.

- The light source board should have all the components placed in one PCB.
- The light source board should be able to handle different LED footprints.
- The light source board should be able to control the trigger of a camera.

2.2.1. Research stage

There were three main topics identified in the hardware design of the boards, those topics were:

- LED brightness control based on the nominal current of the LEDs.
- Communication interfaces between boards.
- Multiple available footprints in the high-power LEDs.

LED brightness control based on the nominal current of the LEDs

The typical way of ensuring a LED current is with a series resistor [Narra and Zinger, 2004], on Fig 2-10 there is a picture of this circuit. Controlling the current of a LED with a resistor is easy to implement; however, it has some disadvantages, which make this circuit not convenient for high power LEDs. The principal disadvantages of using this technique are:

- The resistor dissipation is proportional to the current of the LED, which means that a high current on the LED results in a high dissipation in the resistor.

- Low efficiency in the circuit because the resistor dissipates all the unnecessary power in heat.
- The resistor and LED have some tolerances values, which causes deviation in the actual current.

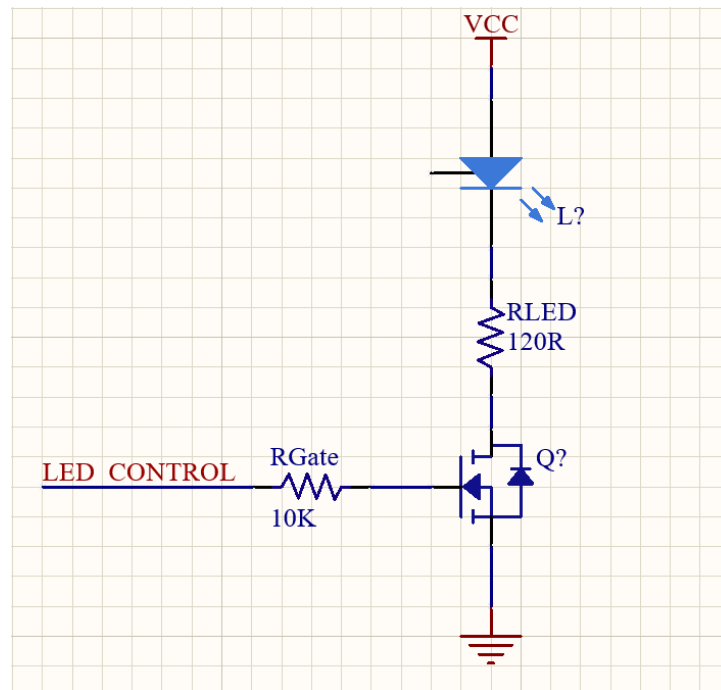


Figure 2-10.: First LED current control circuit.

The second circuit researched was a constant-current driver formed by two transistors as is shown in [LEDnique, 2022]. On Fig 2-11, there is a schematic representation of the circuit. This option solves the problem of ensuring the nominal current of the LEDs, although the problems of low efficiency and high dissipation of the first option will persist. Therefore, this option was discarded because only one advantage was found.

The third researched circuit uses a specialized LED controller IC; it acts like a switching DC-DC converter with special features for LEDs ([ST, 2021]). The circuits use an inductor to change the DC voltage level needed for the LEDs ([Ejury, 2013]); the inductor will store energy increasing the efficiency of the circuit. Some controllers have a dim feature for the LEDs. This characteristic allows the IC to change the brightness using a PWM control signal. Those IC have been widely used for LCD backlights.

Communication interfaces between boards

Wired communication was preferred over wireless because of the complexity of the firmware design [Moscibroda and Wattenhofer, 2006]. There are three primary interfaces available in

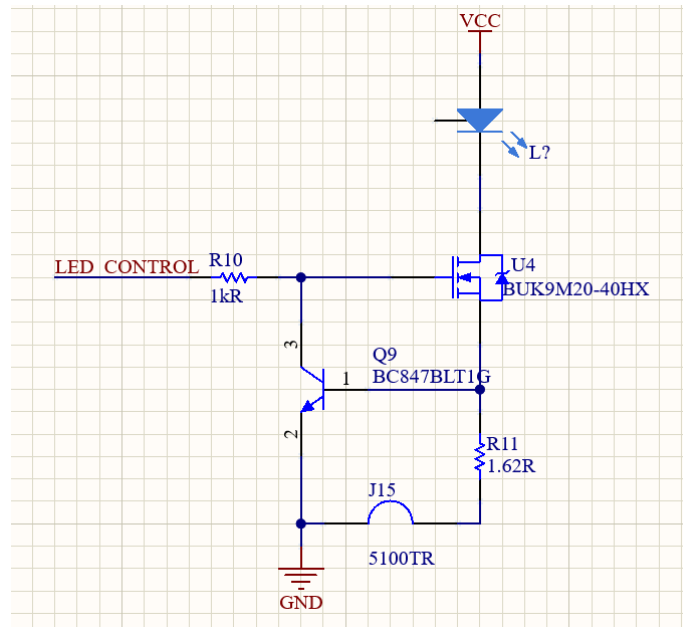


Figure 2-11.: Second LED current control circuit.

wired communications UART, SPI, and I2C. Two of the main factors that will affect the selection of the communication interface are the baud rate and the length of the signals. The UART is a communication interface easy to be implemented, and with hardware adjustments, this communication interface will go through meters of distance [Pini, 2023]. The SPI communication has a greater baud rate than the UART because of the use of a clock signal to synchronize the communication. However, this communication interface will present a problem at large distances due to the frequency of the signals([John, 2022]). I2C is a master-slave communication, its main difference regards to SPI is that it is not full-duplex; in terms of distance, I2C has the same issues as SPI. The light source boards may have more than 1 meter of distance; for that reason, UART was the type of communication selected for this application.

Multiple available footprints in the high-power LEDs

There is no standard footprint for High-power LEDs. They can vary depending on the wavelength of the LED and the manufacturer. Research on the three more common LEDs was done; getting the footprints that can be seen in the datasheets ([LED, 2022b], [LED, 2022c], [LED, 2022a]). Two different groups each with two different footprints were added, they can be seen in Fig **2-12**

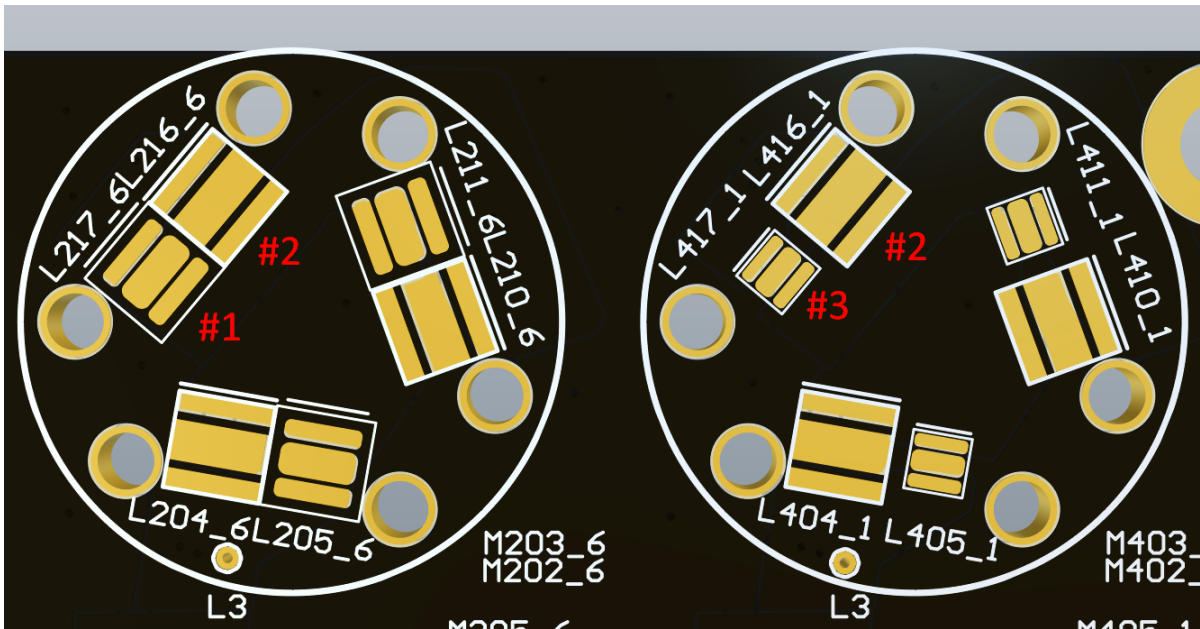


Figure 2-12.: Double footprint LED implementation.

2.2.2. Implementation

Based on the requirements and the researched topics, the following configuration were actually implemented into the board.

LED controllers

The first hardware implementation was the typical LED plus resistors; even if it is not an efficient solution; because of the simplicity, this option was left on the board as a secondary option. The resistors selected were calculated based on the forward voltage of the LEDs and their nominal current. Fig 2-13 shows the implementation in Altium Designer, the resistor with the label TBD defines the nominal current for the LEDs.

The second implementation was the IC LED controller. The IC selected was: [FL7760BM6X](#) ([Onsemi, 2022]). This is a buck controller with high switching frequency LED Driver. It can set the brightness of a LED between 5% to 100% using a PWM external signal. The IC adapts an hysteretic controller scheme that regulates the LED current by sensing the voltage across an external high side sense resistor stabilizing the LEDs nominal current. The schematic diagram of the IC recommended by the manufacturer is shown in fig 2-14.

The additional components of the IC controller were selected based in the recommendations given by the manufacturer. The IC's datasheet describes the main requirements of those components. The needed components were:

- n-channel Mosfet transistor

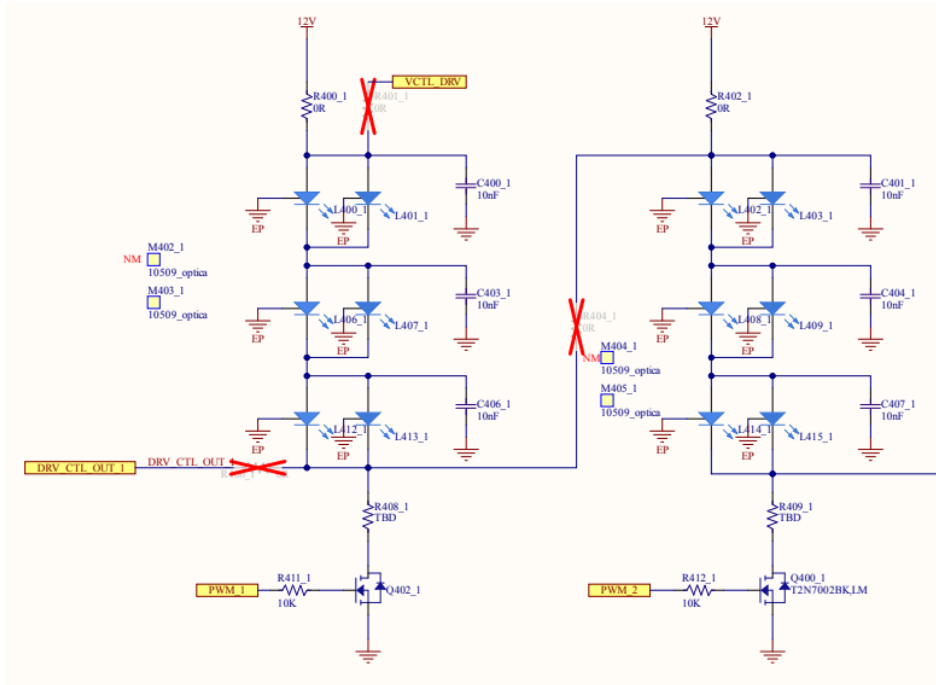


Figure 2-13.: Reconfigurable LED current control using series resistor.

- Sense resistor
- Inductor
- Diode

The two main parameters analyzed in the N-Mosfet transistor were: drain to source resistance which defines how much power dissipates the transistor, and drain to source voltage which restricts the maximum powering voltage for the LEDs. Based on those requirements, the selected MOSFET was TSM2302CX. ([SEMICONDUCTOR, 2022]). The sense resistor value was calculated with the equation given by the datasheet of the controller based on the nominal current needed for each wavelength. The inductance value selected was the recommended value suggested by the manufacturer ([Onsemi, 2022]). The schematic design in Altium Designer is shown in Fig 2-15

Communication between boards

On the board were placed two connectors, one per each external board connected. Each connector has mapped A UART line from the MCU and four GPIOs; the UART line is used for communication, and the four GPIOs are used for synchronization purposes in the firmware. The final implementation of those channels can be seen in Fig 2-16.

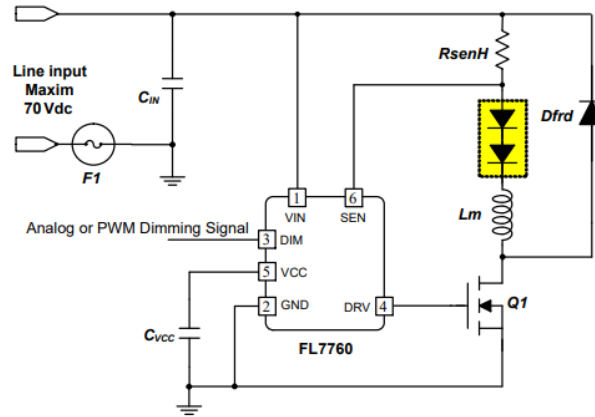
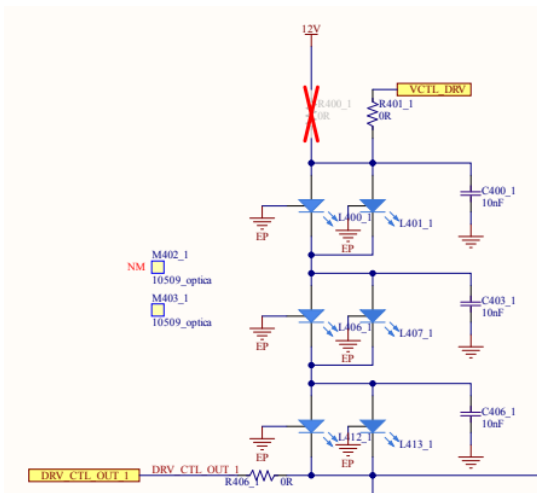
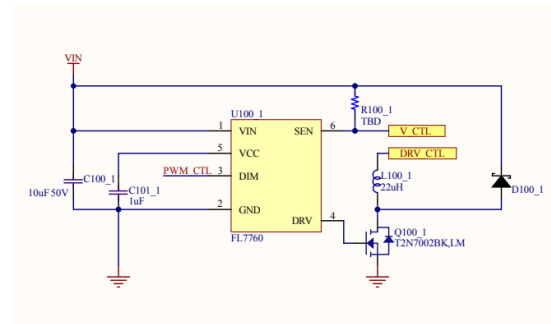


Figure 2-14.: FL7760 recommended schematics [Onsemi, 2022].



(a) LED schematic.



(b) IC controller schematic.

Figure 2-15.: Reconfigurable LED current control using the FL7760 driver.

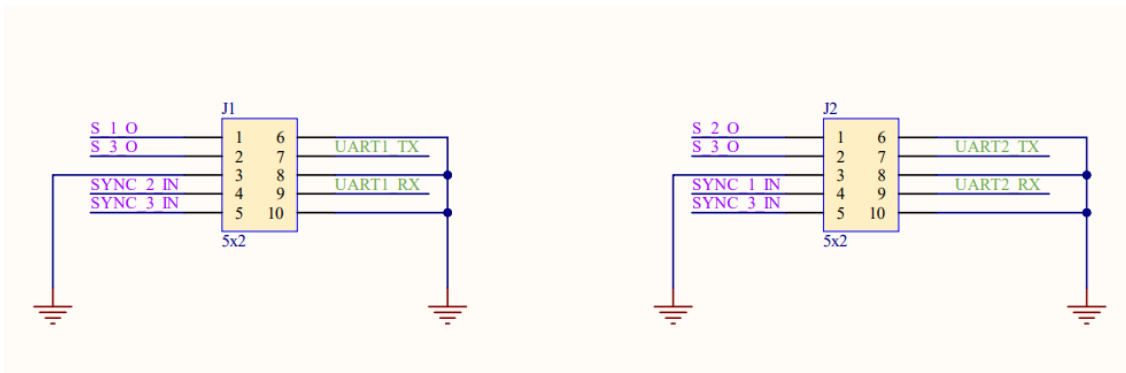


Figure 2-16.: External board connectors pinout.

3. System integration and firmware design

The multispectral enclosure was designed to have up to 8 independent light sources; each of them is able control eight different wavelengths. Depending on the study case, the amount of light needed can change. For this purpose, a driver IC with the feature of controlling the brightness of the LEDs was selected. This IC need a PWM signal from the MCU, which was generated by firmware using hardware Timer peripheral from the MCU to reduce the CPU load.

The communication was planned to be in cascade, which means that each board was in charge of ensuring the correct delivery of the message to the next board in the sequence. With this method, each board only needs to confirm that the next board has received the message. This algorithm reduces the CPU load because each board only waits for one ACK. Cascade connection allows the use of a protocol communication with ID numbers. The communication begins in the board that is connected to the PC (user). This first board is know as the master board and its ID number was assigned to be 0. The ID number begin to increase in steps of one per each board connected in the sequence. The synchronization GPIOs allows each board to know if another board is connected in the sequence.

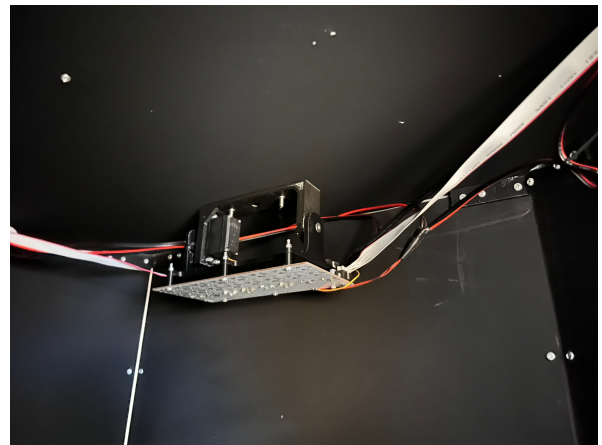
During the assembly process, the cabling was carefully placed to avoid interference with the captures. During the process, no collisions were detected into the system. Finally, the system was tested through commands programmed in the MCU; those commands were created for the interaction between the user and the multispectral system

3.1. System Integration

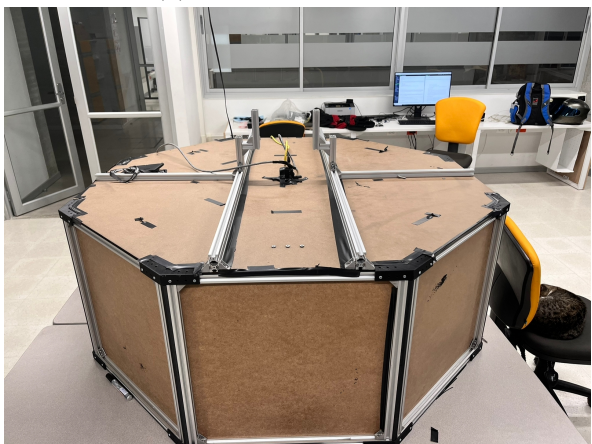
The mechanical parts designed by the dynamics maker team were created, and the MDF walls were painted according to the manufacturer's paint instructions. With those parts, the enclosure was assembled. The light source boards were installed inside the enclosure with their respective motor for moving the board's angle. The cables inside the structure were carefully placed to avoid any interfering with the capture as can be seen in Fig 3-1b. The final system integration assembly is shown in Fig 3-1.



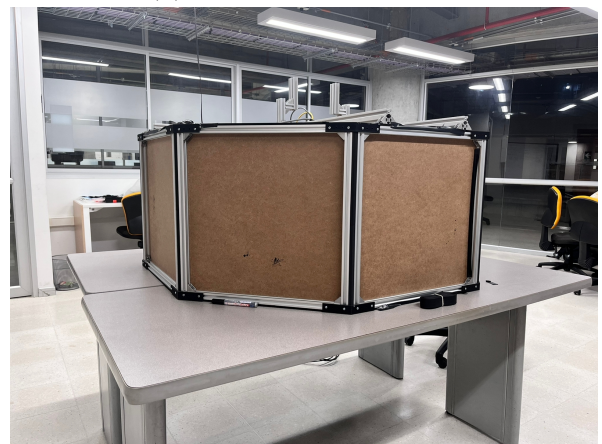
(a) Inside dome capture.



(b) Inside dome capture 2.



(c) front dome image.



(d) side dome image.

Figure 3-1.: Dome images

3.1.1. Electrical connections

In Fig 3-2, there is a representation of how the system is connected. A user PC, a camera and four light boards were mounted in the system. The user's PC is connected to the first board, and each of the slave boards is connected sequentially. The board's firmware was designed to receive a message from the left connector and resend the message by the right connector, so the electrical connection was made following this principle as shown in Fig 3-3.

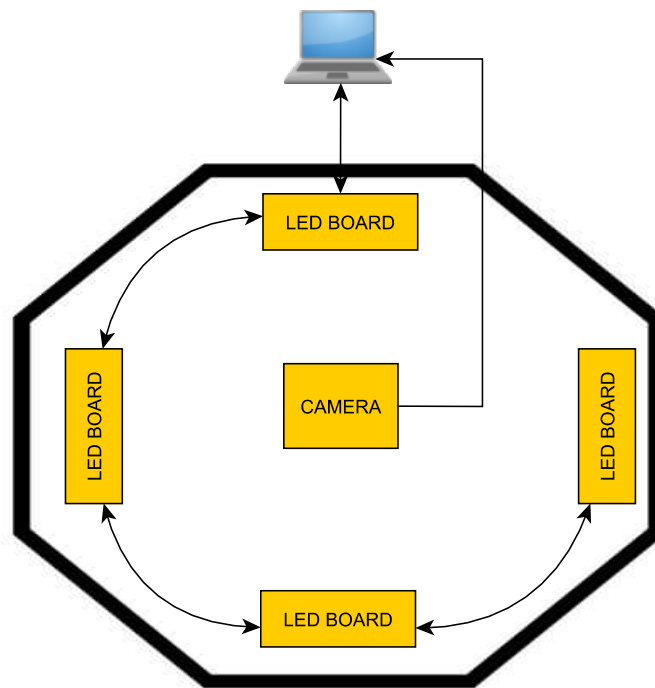


Figure 3-2.: Dataflow block diagram.

3.1.2. Camera trigger

The camera Flea3 GigE [Grey, 2022] has the ability to be triggered by software or hardware, by software the computer is in charge, and by hardware an external device perform control. In the design, we found that the best way is to trigger the camera by hardware and assign this task to the light source board, in that way it will manage the synchronization of the system. The parameters of the camera need to be configured by software. The circuit used for the camera trigger is shown in Fig 3-4.

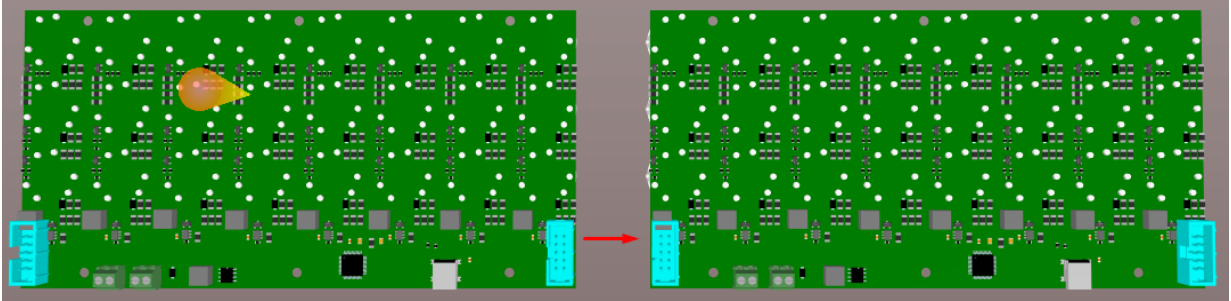


Figure 3-3.: Board diagram connection. Blue connectors were used for board communication.

3.1.3. User to master board communication

A user can communicate with an MCU through the USB port of the PC. There are some MCUs with the hardware to be connected directly to a USB; other MCUs need a UART to USB converter to accomplish this task. The MCU selected has the USB hardware internally; in this way, no external hardware was required. The internal USB hardware of the MCU established the communication between a board and the PC. The baud rate was selected to be 115 200 which is reasonable with low data loss regarding distance [Gupta, 2019].

3.1.4. Master to slave board communication

The communication protocol between boards was based on a cascade connection. The structure of the communication designed can be seen in Fig 3-5. Notice that each board verifies the correct delivery of the message to the other boards in the sequence and only confirms that it gets the message when it knows that all the other boards that continue in the sequence have received the message. It is worth mentioning that each board uses the synchronization GPIOs to know when there is a board connected to them.

3.2. Firmware architecture

The firmware of the boards was constructed into two main stages: identification and execution. In the identification stage each board waits to define the role (as a master or slave board). Then, in the execution stage, the board will execute commands from other boards or from the user depending on the role in the system. In Fig 3-6, there is a diagram of the firmware architecture.

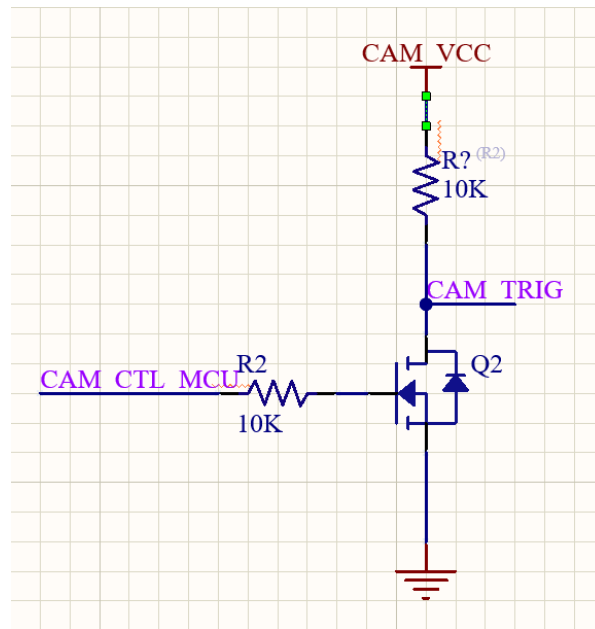


Figure 3-4.: Trigger control circuit.

3.2.1. Identification stage

The architecture used for the connection allows us to identify two types of boards. The first one will be the board connected to the user known as the master board, and the second will be the remaining boards in the sequence known as slave boards. The functions of the master board are:

- Receive and interpret the command sent by the user through the USB port.
- Transmit commands from the user to the slave boards when necessary.
- Control the camera trigger.
- Synchronize all the light sources during a capture.

The firmware and hardware were designed with the flexibility that allows a board to be a master or a slave. Therefore the firmware is the same for all the boards. The firmware defines a master board when a USB connection is detected. The slave boards will know they are slave boards because the master board will use the synchronization pins to let them know that there is a master board already defined. The system was designed to manage up to eight boards connected in cascade mode. As the user needs to be able to send commands to a specific board, an algorithm that assigns ID numbers to the boards was created. The algorithm assigns an ID to each board, beginning with 0 (master board) and increasing in steps of one per board connected into the sequence.

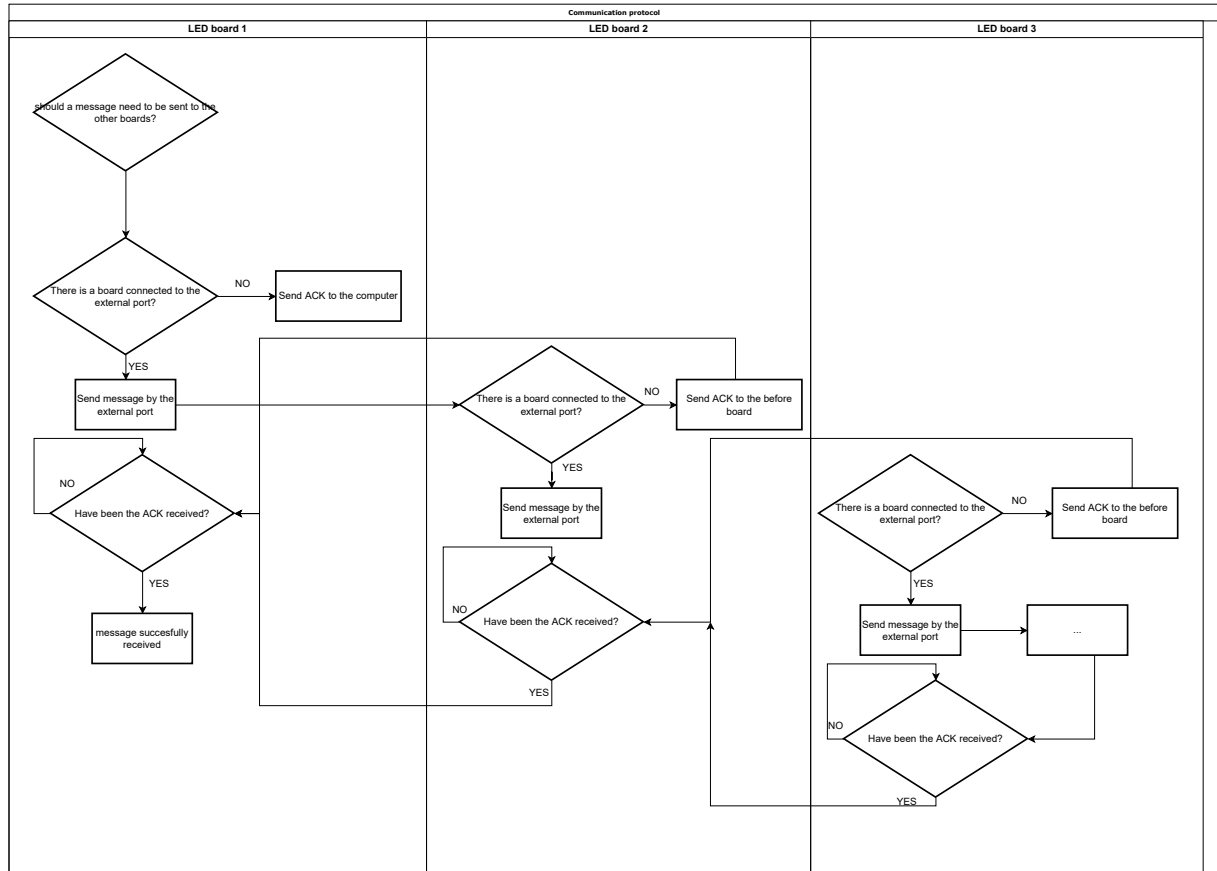


Figure 3-5.: Communication protocol diagram.

For assigning an ID to each board in the system a SCAN command was created to implement the algorithm mentioned above. The assigned ID sequence is depicted in the block diagram in Fig 3-7. The command will look like this “SCAN”, and return to the user the number of boards scanned.

3.2.2. Execution stage

After the boards have been identified using the SCAN command, they pass to the execution stage. In this stage, the boards can receive, execute, and send commands to other boards. The master board is in charge of processing the command received by the user and sending instructions to the slave boards. A queue was implemented into the master board to receive multiple commands simultaneously; the commands are processed in order of arrival. The execution stage of the slave board is less complex than the master board; it receives messages, checks if a process needs to be done with the message, and re-sends the message if there is another board connected in the sequence.

A list of commands was defined for the user’s interaction with the system during the execution

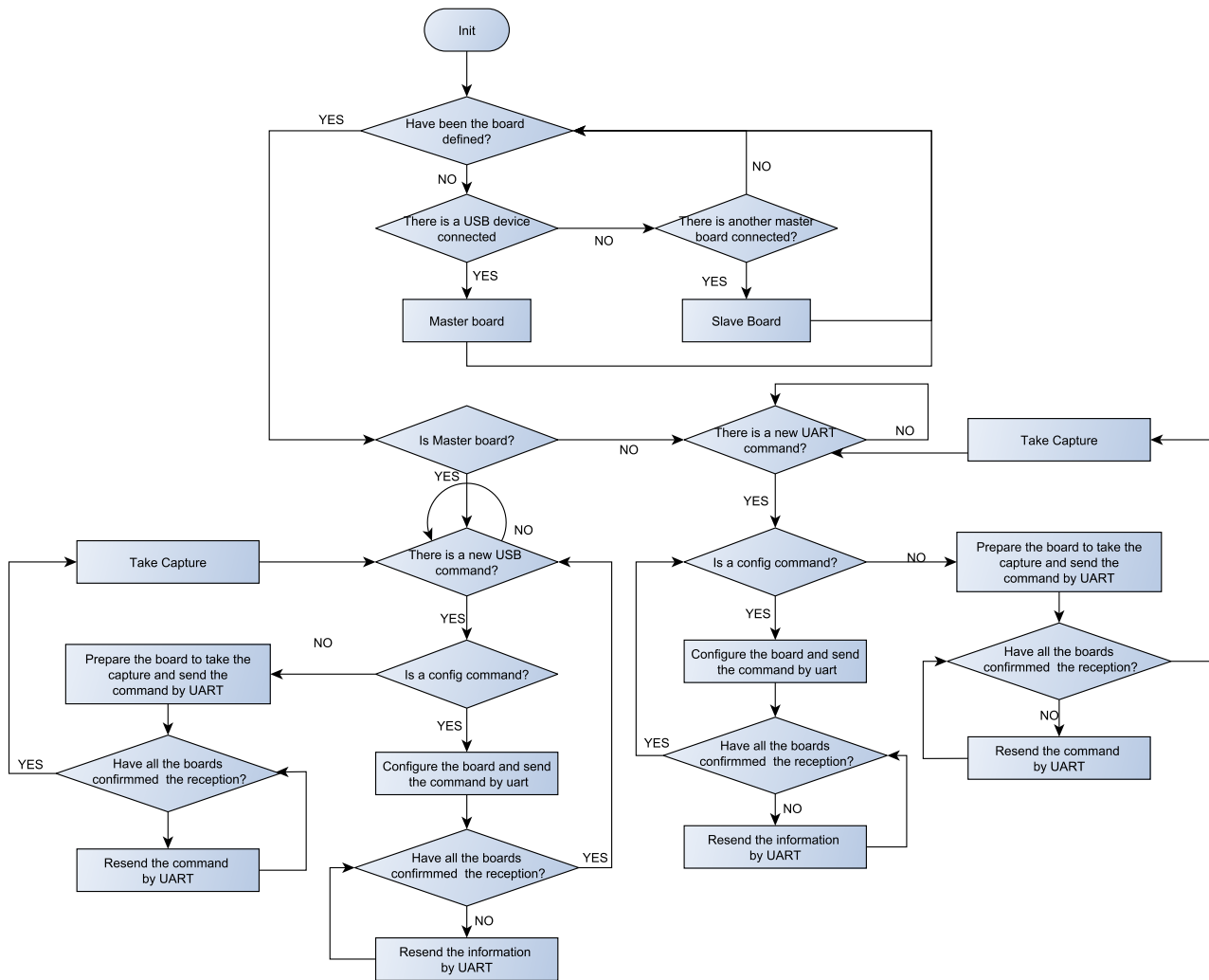


Figure 3-6.: Firmware flow chart.

stage; without them, the user can not execute any action with the multispectral system. The defined commands can be divided into local and global commands. The local refers to instructions specific to each board; those commands need to have the information of the board to configure. The global refers to commands that are common for all the boards (like a broadcast message in networking [Sun et al., 2000]); with those commands, the user does not need to refer to a specific board.

The structure of the commands begins with “{” followed by the command and finished with “}”; If the commands need to have a parameter, the symbol “:” has to be used inside of the command. For example, in “{DUTY:50},” the command is DUTY, and 50 is the parameter. If needed, more than one command can be written in the same line, they should be separated by the symbol “,”; for example, {LED:1,START} has two commands to be executed. When

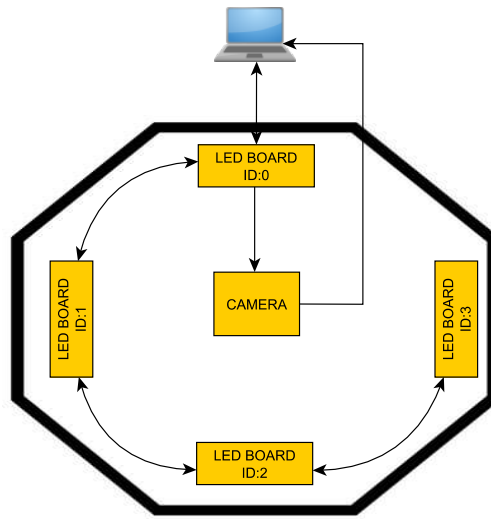


Figure 3-7.: ID diagram distribution.

using local commands and extra parameter with the ID number that should be sent, it will look like “{ID:x}” where the x is the identification number of the board.

The configuration commands programmed were:

- Scanning process to assign an ID number to each board present in the system (SCAN)
- Angle of the board in the structure (ANGLE:xxx).
- LED selector (LED:x).
- Duty cycle of each wavelength LEDs (DUTY:xx).
- Number of ON-OFF times of the LEDs during a capture (FL:x).
- ON time per flash of the LEDs(TL:xxxx).
- exposition time (TO:xxxx).

Board angle command

The servo-motor selected for controlling the position of the lights needs a PWM signal to set the required angle ([ETC, 2022]). For this purpose a PWM channel of the MCU was used. The value of the PWM (Angle) can be set with the word command “ANGLE”. This is a local command, which means that the ID command needs to be also present for selecting the board to configure, the command will look like this “{ID:y,ANGLE: xxx}” where xxx is the angle between 0 and 180, and y refers to the ID of the board to be configured.

LED selector command

In the firmware a LED selector command was implemented. This command lets the board know which can be the LED used for the following configuration or capture commands. The word used for this command is “LE” and the command looks like this “{LED:x}” where X is a number between 1 - 8 (1 = 451nm, 2 = 850nm, 3 = 660nm, 4 = 620nm, 5 = 525nm , 6 = 740nm, 7 = 500nm, 8 = 550nm) referring to the position of the LEDs in the board; the numeration can be seen in Fig 3-8.

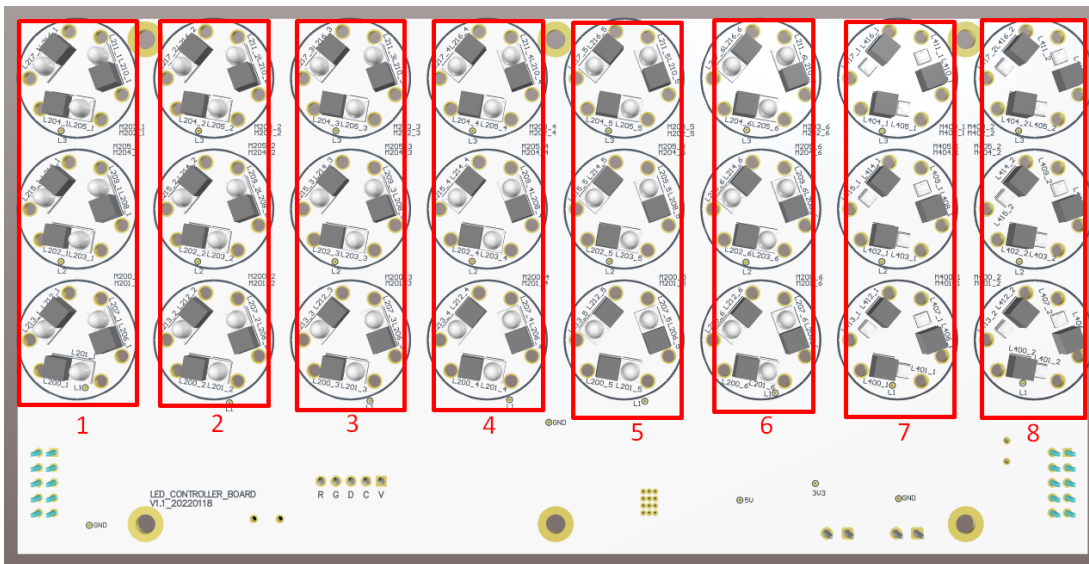


Figure 3-8.: LED number distribution.

As mentioned before, after sending, for example, “{LED:3}” all the next configurations or captures will be applied with the LED number 3.

Duty cycle command

On the boards, each wavelength is connected to a different PWM output for controlling the light intensity in the scene. This allows the board to configure each wavelength independently. The command must be sent after the LED selector command to define the wavelength to be configured. The duty cycle is a global command, meaning that if wavelength 1 is configured to a specific value, wavelength 1 of all the boards will be configured to the same value. When a user needs to configure a different duty cycle on the same LED in a different board, he or she will need to change the duty cycle value before doing each capture. The word used for this command is “ DUTY”, and the command will look like this “{LED:y,DUTY:xxx’ where the xxx is the duty cycle between 0 and 100 and y is the wavelength to be configured between 1 and 8.

3.2.3. Multiple ON-OFF wavelength times command

In some capturing scenarios, the user will need to turn ON-OFF the wavelength multiple times. The board can do this with a parameter known as number of flashes (`#FLASHES`). This can be set with a value between 1 and 10. When using this feature, the firmware takes the total exposure time and divides the quantity of the flashes into equal intervals of time. For the correct operation of this feature, the following condition needs to be accomplished: $\text{LED ON TIME} \times \text{\#FLASHES} < \text{EXPOSURE TIME}$. This is a global command; in that way, all the boards will have the same `#FLASHES` configured. The word command used is “FL” and the command will look like this “{FL:x}” where x is the number of flashes between 1 and 9.

ON time command

For different applications it is essential to change the on time for each group of LEDs. In some cases, a short time is needed, and in other cases, a longer time. The on time of the LED can be configured on all the boards, and it applies to all the wavelengths of the board. This is also a global command, meaning that it will be the same for all the boards in the system. The word command used is “TL”, so the command will look like this “{TL:xxxx}” where xxxx is the on time of the LEDs in milliseconds and can be a number between 1 and 9999 milliseconds.

Exposure time command

According to the LED on time and flashes, the exposure time needs to be changed. This is a global command which will be applied to all the boards of the system. The word command used for this purpose is “TO” and the command will look like “{TO:xxxx}” where xxxx is the exposure time of the camera and can be a number between 1 and 9999 milliseconds. (TO after *Tiempo de Obturación* in Spanish).

Capture command

To perform a capture, the word “START” is used. This command needs to include the boards to do the capture because it can be one or more boards at the same time. The wavelength that will do the capture also needs to be specified, if not the system will do the capture with the last wavelength selected. In addition, the duty cycle of the wavelength can be changed, again if it is not configured, then the capture will be performed with the last settings. An example of a capture with only one board is “{ID:x,LED:y,DUTY:z,START}”, and a command with multiple boards at the same time looks like this “{ID:x,ID:t,...,LED:y,DUTY:z,START}”

The camera needs to be configured for triggering by hardware to run the capture command. This configuration shall be done through a PC. The camera has some configurable GPIOs, which can be seen in Fig 3-9; the GPIO number two was selected as the hardware trigger.

In the hardware triggering mode, the camera will begin the exposure with a low level pulse sent by the MCU and will continue during all the time while the MCU maintains this low pulse.

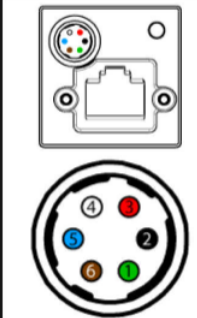
Diagram	Color	Pin	Function	Description
	Green	1	Power	+12 V DC Camera Power
	Black	2	Opto Input 1	Opto-isolated input
	Red	3	NC / +3.3 V	+3.3 V output. Current 120 mA (nominal). Firmware enabled
	White	4	Opto Output 1	Opto-isolated output
	Blue	5	Opto GND	Ground for opto-isolated I/O, not connected to camera ground
	Brown	6	GND	DC camera power ground
To configure the GPIO pins, consult the General Purpose Input/Output section of your camera's Technical Reference Manual.				

Figure 3-9.: Camera port pinout [Grey, 2023].

3.3. Light source calibration values

Before initiating a capture process is important to define the next configuration parameters:

- PWM value of each LED.
- Exposure time.
- Number of flashes.
- ON LED time.
- Angle of the boards

Before initiating the captures, those values need to be defined. For this purpose, a calibration algorithm was developed to get adequate PWM values based on a defined angle, #FLASHES, ON LED time, and EXPOSURE TIME. This algorithm uses a white object with a 70 % of reflectance. If the software cannot find the PWM values that yield captures with 70 % after the sweep, then the exposure time and ON LED time must be adjusted. A way to know how to change those parameters is: if the image never reaches the 70 % of intensity, the ON LED time needs to be increased, and if the problem is that the reflectance change abruptly between steps of only 1 % of the PWM means that the ON LED time is too large and then needs to be reduced.

The light source calibration process needs to be updated for each angle to be used in the capture. This process must be performed periodically because the LEDs and camera will reduce its performance and lose accuracy over time.

4. Multispectral image acquisition and dry matter extraction

Before beginning with data acquisition, it was essential to ensure the proper function of the system. Therefore, objects like Color-checkers and avocados were captured to verify the system functionality.

In the experiments, 14 avocados that were commercially available were used to construct a small database containing both multispectral images and their corresponding dry matter (computed following the technique in [Carvalho et al., 2015]).

Since the inner surface of the avocado is reflective and concave, the images exhibit lighting issues mainly due to shadows pertaining self-occlusions and specular reflections. Hence, a synthetic image was conformed by selectively averaging the information coming from different images, each one of them containing the subject under a light source of a fixed wavelength but diverse incident angles. In the Chapter, I show how the technique developed enabled us to reduce the aforementioned effects significantly.

Masking images help us focus in the pixel data that contain relevant information in the capture. Therefore, a mask was applied to remove the areas in the images that do not yield usable avocado information (mostly image background).

Histograms were used to see the pixel values of the different avocados. Histogram graphs allow a quantitative representation of the data; in an image, it helps us to see the distribution of the pixel values. The histograms allow us to infer information that highlight, to some extent, different ripening states.

4.1. Image acquisition

Once the system was up and running, some images were captured to check the correct behavior of it. In Fig 4-1, there is a picture of the color checker taken with the different wavelengths. Each channel shows the reflectance response of the scene under its corresponding wavelength. In Fig 4-2, a RGB representation of the color checker is illustrated.

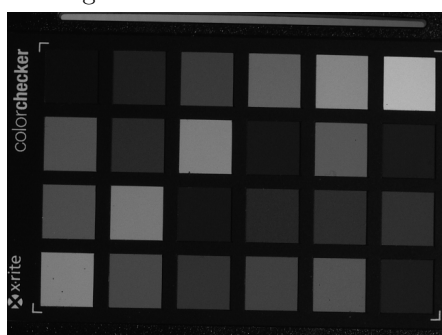
The second test was carried out using a scene with an avocado. In Fig 4-3, the reflectance of the avocado under lights of different wavelengths is presented. Notice that the concave nature of the avocado insides introduce shadows, generated by self-occlusions seen from the LED incident direction.



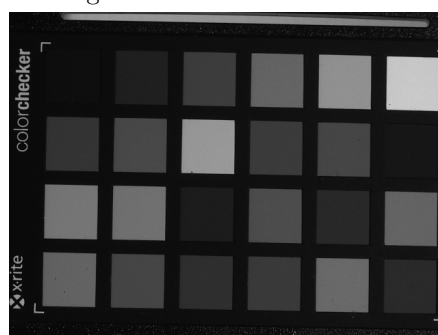
(a) Color checker under 451 nm lighting.



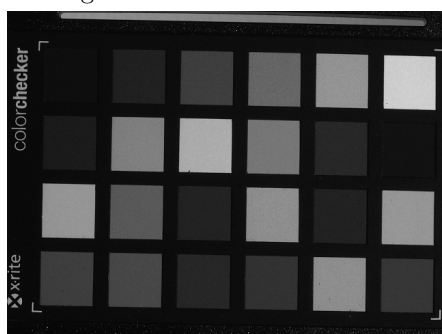
(b) Color checker under 500 nm lighting.



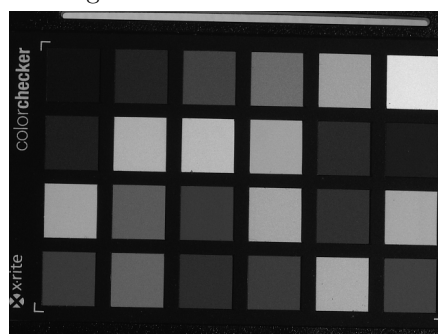
(c) Color checker under 525 nm lighting.



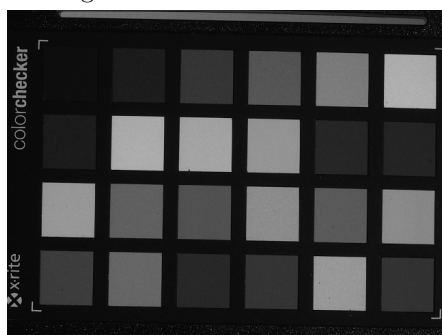
(d) Color checker under 550 nm lighting.



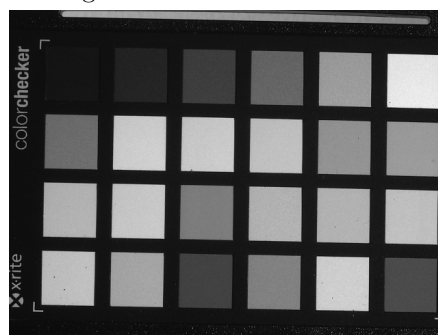
(e) Color checker under 620 nm lighting.



(f) Color checker under 660 nm lighting.



(g) Color checker under 740 nm lighting.



(h) color checker under 850 nm lighting.

Figure 4-1.: Color checker images under different lighting.

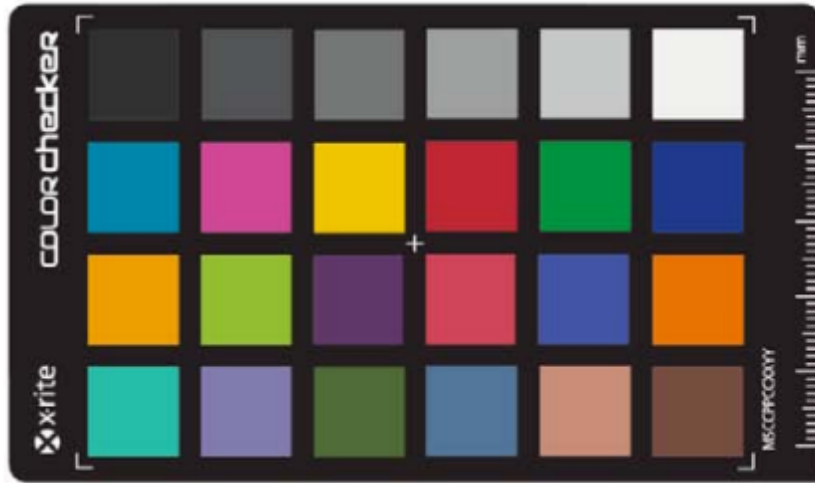


Figure 4-2.: Color checker RGB image.

Histograms are tools that allow us to see the distribution of the intensities found in an image. In this work, the histograms of the eight images corresponding to the different wavelengths were used to compare the information obtained using different avocados. On the histogram graphs, each channel represents the reflectance to a specific wavelength. For example, in Fig 4-4, the histogram representation of two avocados in different ripening states are shown. As expected, there are differences between the histograms, indicating that it is possible to approximate the ripening state by the means of the reflectance.

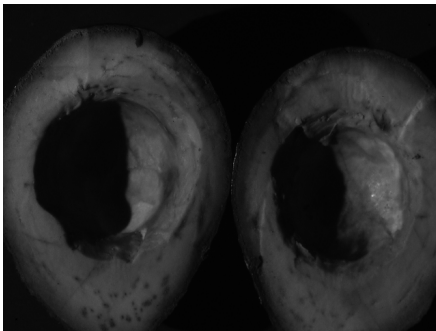
4.2. Dry matter in avocado

As shown in [Carvalho et al., 2015], there is a relation between the dry matter of an avocado, and the appropriate moment to be harvested down from the tree. Furthermore, based on the document [Lyu, 2019], there is a possibility of finding a relationship between the dry matter and the information obtained from multispectral captures. On that article, the chart shown in Fig 4-5 was published. The image shows the principal wavelengths with the most significant differences. Those wavelengths are 550 nm, 660 nm, and 790 nm. In the light source boards, wavelengths close to those mentioned in the article were chosen, hoping to obtain valuable information from them.

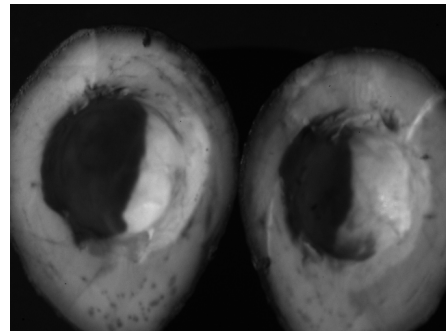
4.2.1. Dry matter extraction method

The people who work with avocados use an invasive extraction method to calculate the dry matter. According to [Carvalho et al., 2015], we followed the process below:

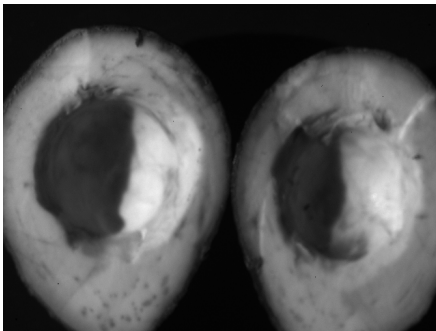
- The avocado was cut in the middle into two halves.



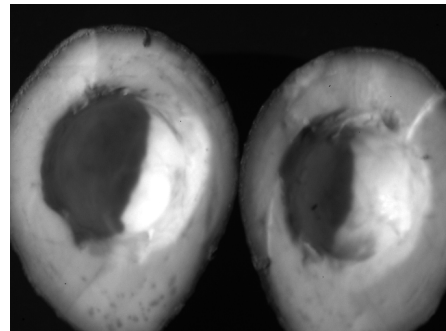
(a) Avocado under 451 nm lighting.



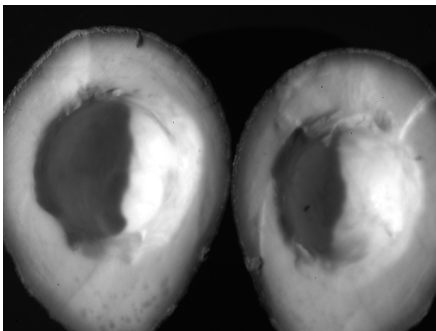
(b) Avocado under 500 nm lighting.



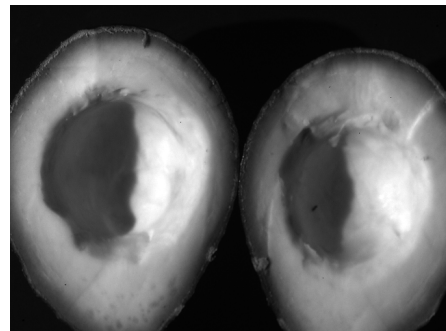
(c) Avocado under 525 nm lighting.



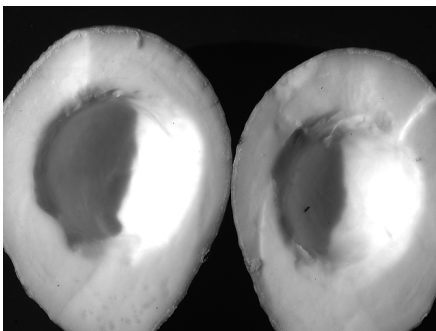
(d) Avocado under 550 nm lighting.



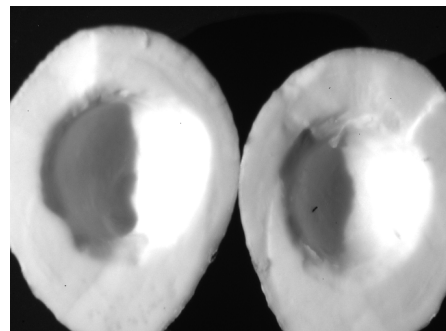
(e) Avocado under 620 nm lighting.



(f) Avocado under 660 nm lighting.

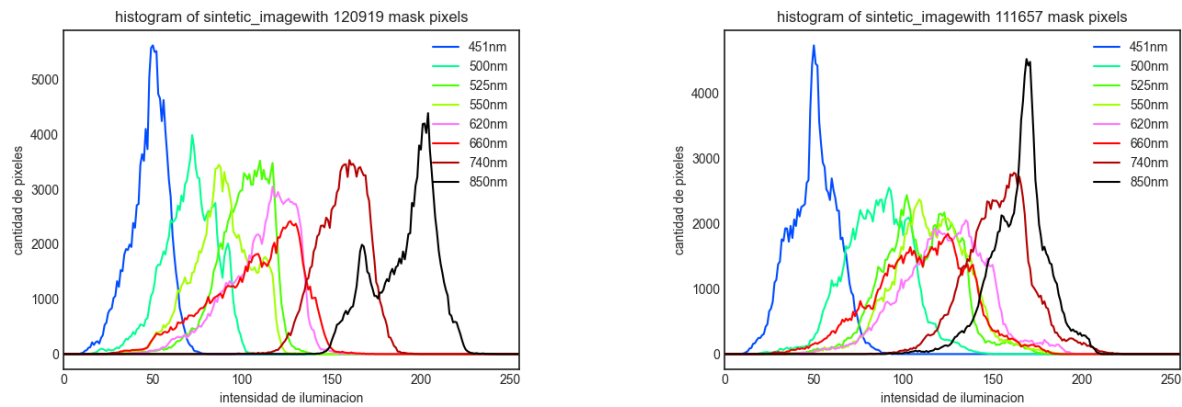


(g) Avocado under 740 nm lighting.



(h) Avocado under 850 nm lighting.

Figure 4-3.: Avocado images under different lighting.



(a) Histogram of the first avocado captured.

(b) Histogram of the second avocado captured.

Figure 4-4.: Histograms of the first two avocados captured.

- The avocado seed was removed.
- The remaining seed skin left over the inside 'of the avocado was removed with a spoon.
- The peel of the avocado was removed with a potato peeler.
- A small piece of paper was weighted using a balance. Such piece of paper is going to be used as slide to place the avocado sample.
- Slices of the avocado were put into the paper sheet with the potato peeler.
- The weight of the paper sheet with the avocado samples was measured. A minimum quantity of 10 grams was defined to get a better sample, and the final weight was recorded.
- The samples on the slide were put into a microwave oven, and heated during 3 minutes with the oven power configured to 70 %. After this time, the weight of the sample was measured again, and recorded.
- The microwave oven power was set to 30 %, and the samples were heated during 1 minute each time. After this time, the weight was measured again.
- The last step was repeated until the weight did not change more than 0.1 gr.

4.3. Exercise with avocado dry matter

For running classification tests, 14 Avocados were selected. First, avocado images were captured, and then the dry matter values were measured using the invasive method described in

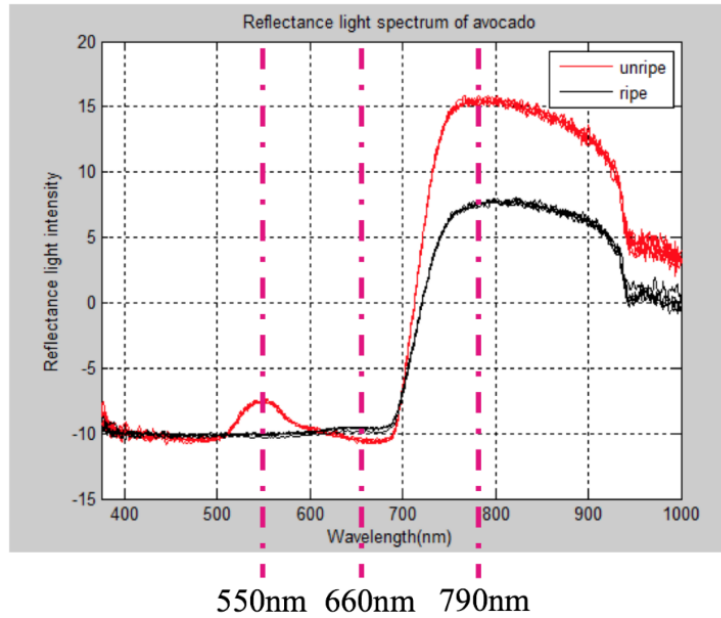


Figure 4-5.: Avocado wavelength reflectance [Lyu, 2019].

the previous section. The process of getting the dry matter of one avocado takes between 10 and 30 minutes per avocado. All the information related to the dry matter extraction of the avocados can be found in Table 4-1. In the experiment, the following pictures were taken:

- One picture per LED wavelength and board, for a total of 24 pictures (8 wavelengths x 3 boards).
- The avocado was captured in two ways, open by the middle and without any cut, as can be seen in Fig 4-6

It is worth mentioning that only three boards were used due to a hardware malfunction detected in the fourth one.

4.3.1. Masking of the avocados in the images

In the captured images, it is essential to separate the pixels which will give relevant information from the pixels that will give little to no information. Similar processes have been done in [Ataer-Cansizoglu et al., 2015], [Doshi et al., 2013], [Bustard and Nixon, 2010]. Two of the main reasons that will make a pixel carry unusable information are the presence of shadows and saturation. The shadows are due to the position of the light source and the concave shape of the avocado. This will cause distortion in the information ([Zhang et al., 2015]). On the other hand, saturation gives no information, which is a problem like in [Eden et al., 2006]. The saturation problem is due to the specular reflection produced in the image, and the blooming effect. More information about it is in [Matusik, 2003].

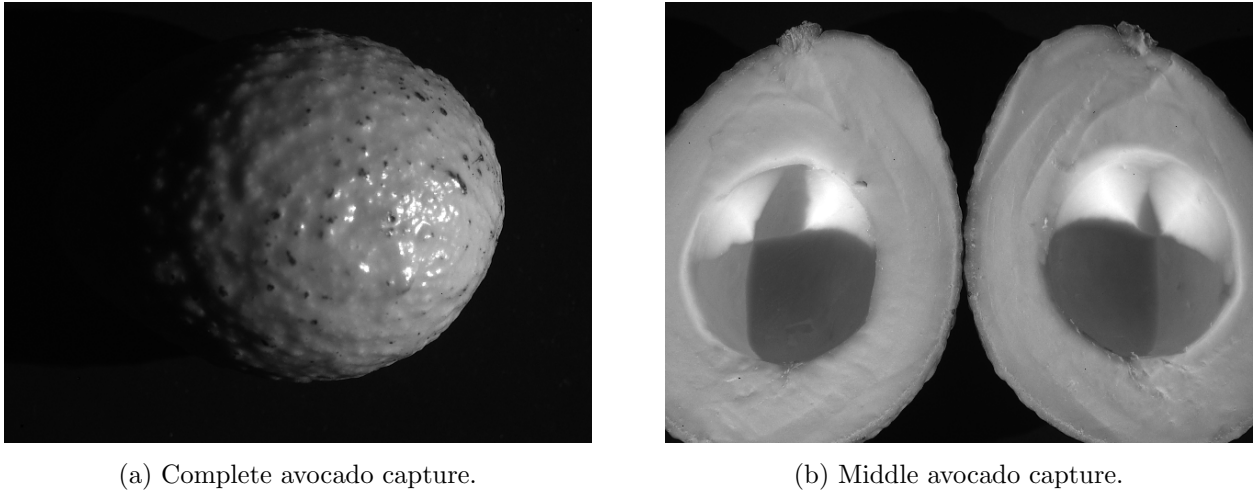


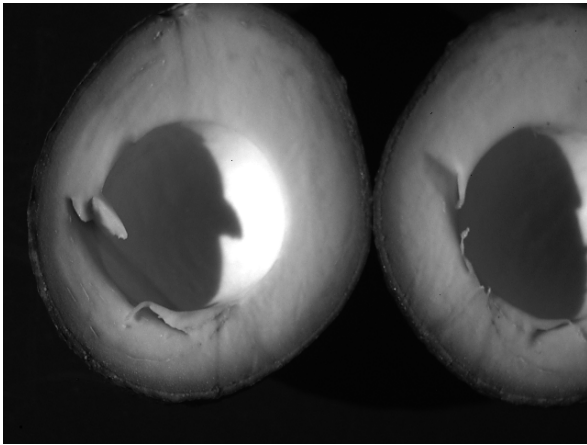
Figure 4-6.: Avocados capture

As a method to decrease the shadows and saturation parts on the image, I have decided to generate a synthetic image with the three captured images, acquired using the three boards. The information contained in the images is complementary since the boards point to the scene from different angles. The synthetic image was generated with the median pixel of the three captured images. The high brightness and shadows in some parts of the picture were solved, as can be seen in Fig 4-7; the shadows of the image were reduced but not totally removed from the image. Similar approaches have been used in [Albin et al., 2002]. The more affected area of the avocado was the area of the seed due to its concave shape. A custom mask was created to remove this area, as well as to focus the regions to be included in posterior analysis. An example of the masks can be seen in fig 4-8

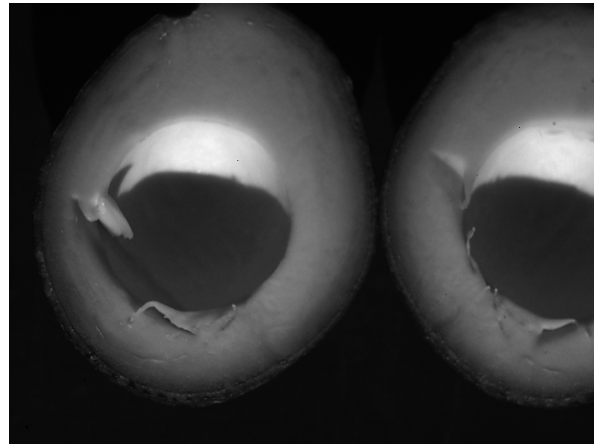
4.3.2. Reflectance normalization

The use of relative reflectance preprocessing was applied in the image to obtain more consistent data in the pixel. This method was also used in [Qin et al., 2009]. On it, the author calculated the reflectance values with the equation 4-1, where R refers to the relative reflectance; R_s is the original value of the pixel; R_r is the value of the camera without any light to measure (it measures the dark current into the sensor); and R_d is the value of a white diffuse reflectance. In the project was used a spectralon for this capture. The spectralon used for the white captures has a reflectance of 99% for all the wavelengths between 250 and 2500 nm.

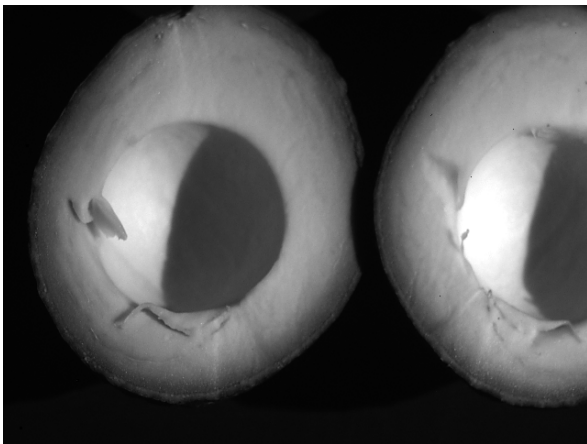
The final value of the reflectance was represented between 0 a 100. on fig 4-9, there is a comparison between the histogram of an original image and its relative reflectance. Based on the histogram differences, there is a change in values after calculating the relative reflectance. This process is necessary to be done, before using those data in any classification process.



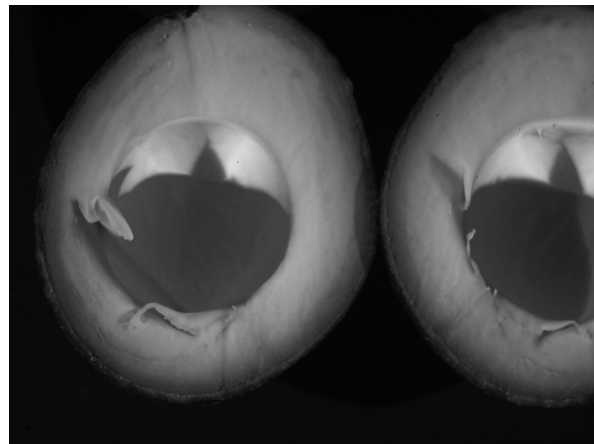
(a) Board 0 with 660 nm light.



(b) Board 1 with 660 nm light.



(c) Board 2 with 660 nm light.



(d) synthetic image.

Figure 4-7.: Avocado synthetic image.

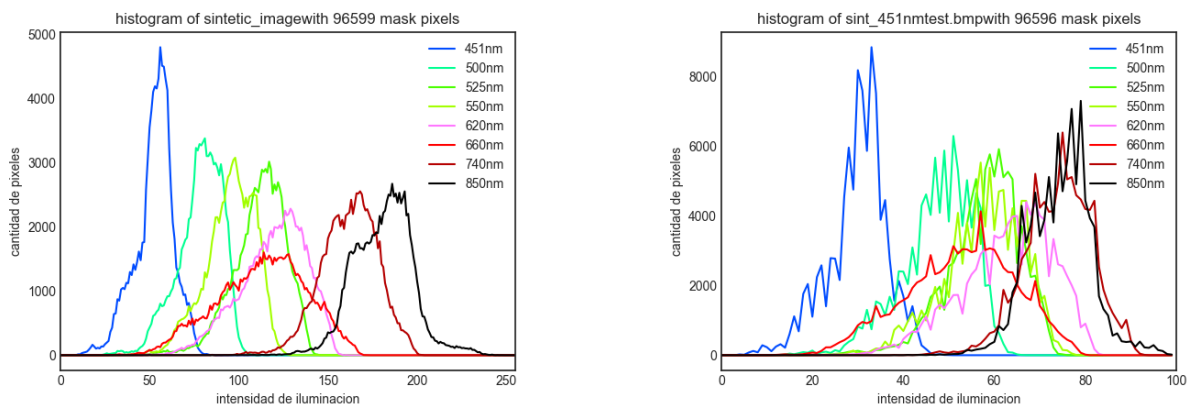
Table 4-1.: Avocado experiments record.

Avocado-sample	sheet weight	sheet + av weight	samp weight after process	Dry matter
1-1	2.362g	17.27g	5.46g	20.78 %
1-2	2.366g	19.807g	5.84g	19.91 %
2-1	2.323g	17.49g	5.12g	18.44 %
2-2	2.331g	17.32g	5.148g	18.79 %
3-1	2.37g	17.516g	4.33g	12.94 %
3-2	2.365g	10.89g	3.65g	15.07 %
4-1	2.299g	17.187g	5.112g	18.89 %
4-2	2.303g	10.515g	3.907	19.53 %
5-1	2.308g	17.301g	4.785g	16.52 %
5-2	2.301g	10.272g	3.47g	14.66 %
6-1	2.315g	17.006g	5.22g	19.77 %
7-1	2.35g	17.178g	4.948g	17.52 %
7-2	2.375g	17.23g	5.203g	19.03 %
8-1	2.32g	17.011g	5.741g	16.48 %
8-2	2.37g	17.331g	4.97g	17.38 %
9-1	2.323g	17g	4.785g	16.77 %
9-2	2.381g	17.239g	4.724g	15.77 %
10-1	2.291g	17.19g	5.028g	18.37 %
10-2	2.301g	17.08g	4.938g	17.84 %
11-1	2.367g	17.361g	5.076g	18.06 %
11-2	2.378g	17.212g	4.932g	17.22 %
12-1	2.319g	17.463g	4.95g	17.37 %
12-2	2.319g	17.039g	5.044g	18.51 %
13-1	2.33g	12.233g	3.99g	16.85 %
13-2	2.328g	12.467g	4.1g	17.48 %
14-1	2.383g	17.139g	5.031g	17.94 %
14-2	2.372g	18g	5.46g	15.122 %

$$R(\lambda) = (Rs(\lambda) - Rd(\lambda)) * 100 \% / (Rr(\lambda) - Rd(\lambda)) \quad (4-1)$$



Figure 4-8.: Example mask used in avocado images.



(a) Histogram of the original image.

(b) Histogram of the processed image.

Figure 4-9.: Histograms of avocado synthetic image.

5. Avocado dry matter results

In the last chapter, the procedure followed to capture and mask 14 avocados was presented. Based on [Lee et al., 1983], it was confirmed that there is a relationship between avocado ripeness and its dry matter. Therefore, this chapter shows the results of a first approximation to tackling the problem of establishing a relationship between the multispectral avocado captures and its dry matter. For this purpose, algorithms like the linear discriminant analysis (LDA), Mahalanobis distance, and self-organizing maps were used.

Before exploring the algorithms, we begin to observe the spatial distribution of the data using visual plots. these plots can only have three dimensions, and the captured data have a total of eight (each dimension per wavelength); for getting the graphs, a dimensionality reduction was applied using PCA. With the obtained graphs was inferred that there is a possible separability between the different avocados.

The first classification exercise was carried out using LDA. This method requires examples of at least two different classes, or prior knowledge of their distributions. In the context of this Thesis, the spectral information contained in the captures taken from seven avocados was used as references. The selected avocados have the following dry matter percentages: 14 %, 15 %, 16 %, 17 %, 18 %, 19 %, 20 %. The dry matter was measured using the technique from [Carvalho et al., 2015]. Then, the spectral information of the remaining seven avocados was used to approximate their dry matter using LDA.

LDA was applied in three different tests. In the first test, each pixel inside of the avocado mask in the multispectral image was classified into one of the seven classes. Then, the mode of the dry matter values obtained was assigned as the final dry matter of the avocado. This method had a maximum relative error of 29.19 %. In the second test, each pixel was classified, and the median of dry matter value values obtained was assigned as the final dry matter of the avocado. this method had a maximum relative error of 29.19 %. Finally, in the third test, the probabilities of each pixel belonging to a class were computed. Then, the two classes with more probability were taken and pondered to define the dry matter value of the pixel. Once the value of the pixel has been computed, the median value of the pixels inside the avocado mask of each image was assigned as the final dry matter of the avocado. this method had a maximum relative error of 21.09 %.

The second classification exercise was done using the Mahalanobis distance. Three different tests were done. The first test begins by assigning the dry matter value of the class with minimum Mahalanobis distance towards each pixel. Then, the median of the dry matter value of the pixels inside the avocado mask was selected as the final dry matter value of the

avocado. This test had a maximum relative error of 21.14%. The second test did a weighted sum between the two classes with the minimum distance for assigning the value to each pixel. The median dry matter value of the pixel was selected as the final dry matter value of the avocado. The test had a maximum relative error of 14.77%. Finally, the third test was a combination between the first and the second, taking into account the two minimum distances only when their respective dry matter are consecutive in the class set. The maximum relative error of this test was 24.43%.

The third classification method used the self-organizing maps (SOM). In this method, the avocado pixels were classified based on the seven-point generated by a one-dimensional self-organizing map. Unfortunately, problems in the border were found after testing this algorithm. A maximum relative error of 17.7% was obtained from this test.

5.1. Visualization of the Spectral avocado information using PCA

The captures acquired using the illumination provided by the eight wavelengths selected are stacked to form an image with a depth of eight dimensions. One can use dimensional reduction techniques in order to depict some information related to the spectral distribution of the data, such as PCA ([Ringnér, 2008]), LDA ([Kim et al., 2007]), Truncated SVD([Speer et al., 2008]). In this work, the avocado information was plotted using projections of the data along the main axes resulting from PCA.

PCA was computed with the aid of the `sklearn.decomposition.PCA` library, which in turn uses singular value decomposition to achieve the dimensionality reduction. More information on the library can be found on [scikit learn, 2022]. In this work, only the main three vectors of PCA were kept in the reduced representation of the data. The projected data was plotted using pairs of coordinates. For example, in Fig 5-1, there is a distribution of the spectral information inside an avocado mask after the reduction. In Fig 5-4, there is the representation of the 14 avocados in the three main dimensions of PCA.

5.1.1. LDA classification and dry matter approximation

LDA is a technique that aims to find the linear projection that maximizes the interclass variation between two classes, while minimizing the intraclass variation of them. On Fig5-3, there is a picture of the main differences between PCA and LDA. Those methods have been used in [Choubey et al., 2020], [Naseer et al., 2016], [Sharma et al., 2006].

The library `sklearn.discriminantanalysis.LinearDiscriminantAnalysis` from python was used to apply the LDA algorithms. This library allows us to make predictions of a new avocado into different avocado classes and the probability of belonging to a specific class. Based in Table 4-1 our samples have a dry matter that ranges between 14% and 20%.

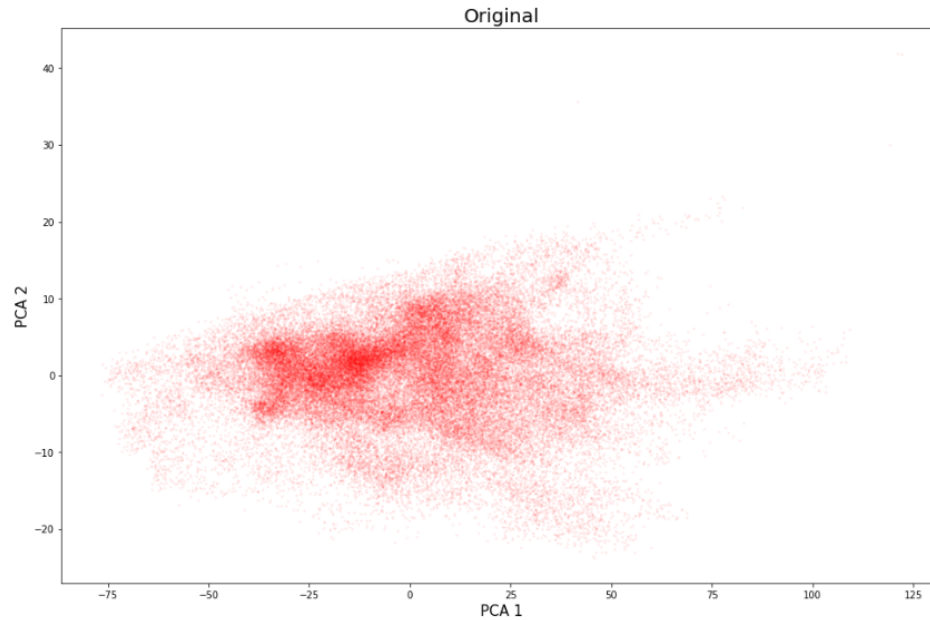


Figure 5-1.: Avocado pixel information after PCA.

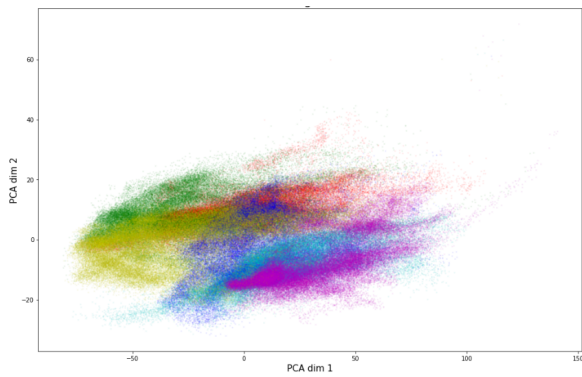
Seven classes were defined within this range, corresponding to dry matters of 14 %, 15 %, 16 %, 17 %, 18 %, 19 % and 20 %. For each class, the closest avocado to the percentage value was selected. Table 4-1 from the previous chapter shows the dry matter values computed from each one of the 14 avocados; from that information, the reference pairs selected are: 14 % = Avocado 3, 15 % = Avocado 5, 16 % = Avocado 9, 17 % = Avocado 13, 18 % = Avocado 7, 19 % = Avocado 4, 20 % = Avocado 1. The distribution plot of the seven classes using PCA can be seen in Fig 5-4.

Three types of classification were done. they have been based in pixel classification as have been used in other works like [Peláez-García et al., 2021], [Atkins et al., 2001], [Sampat et al., 2002], [Myint et al., 2011]. The three types of classification were:

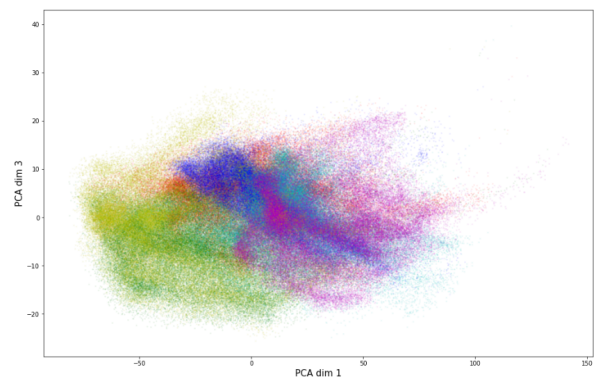
- Pixel classification to class with the statistics mode.
- Pixel classification to class with the statistics median.
- Pixel classification to a class using probabilities and statistics median value.

Pixel-wise classification using the mode

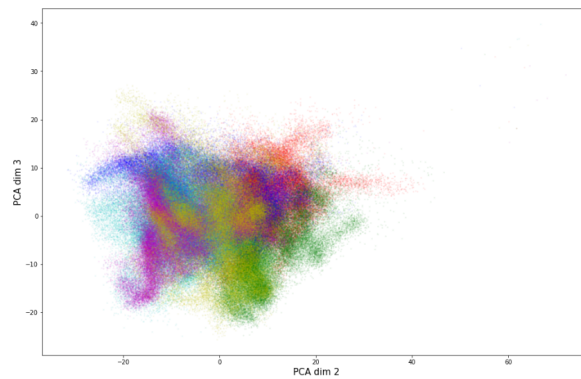
On pixel-wise classification, the pixels of the multispectral avocado image were labeled using one of the seven reference classes. With the confusion matrix ([Room, 2019]), we can see how many pixels were correctly classified and which pixels were wrongly classified. Fig 5-5 represents the pixel classification results of the same reference avocados. From this confusion



(a) Avocados representation PCA Dim 1 Vs Dim 2.



(b) Avocados representation PCA Dim 1 Vs Dim 3.



(c) Avocados representation PCA Dim 2 Vs Dim 3.

Figure 5-2.: Avocados representation after PCA reduction.

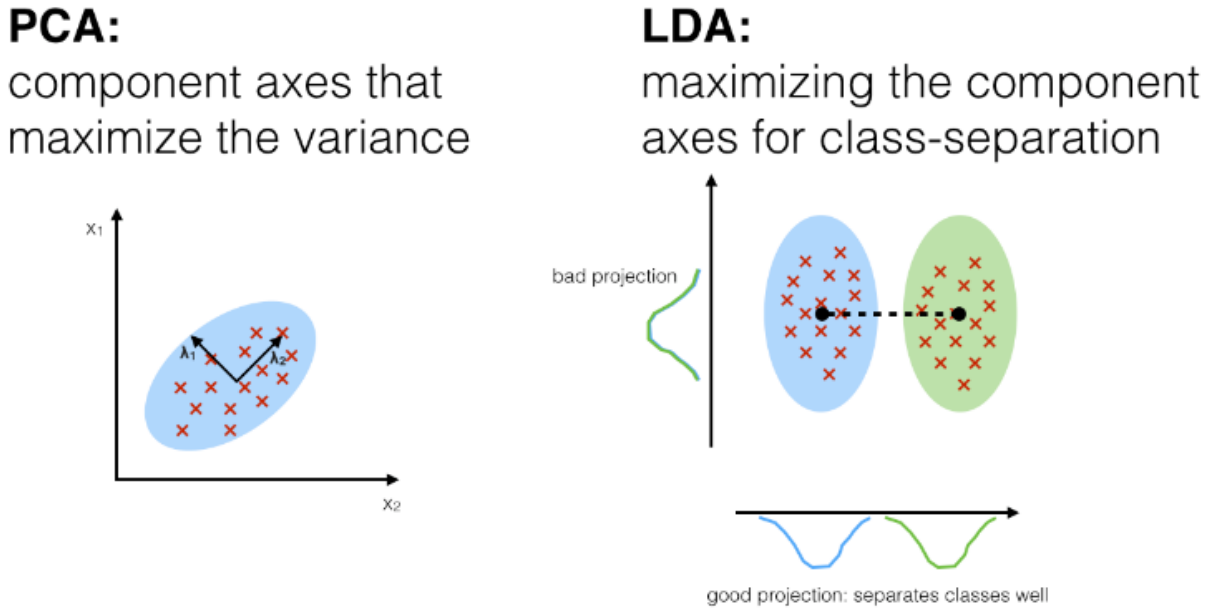


Figure 5-3.: PCA vs LDA differences [Avila, 2022].

matrix, we can infer that the avocado references 14%, 15%, 17%, and 19% have a high percentage of the pixels well classified. For class 16% the error was higher, but the confusion was mainly concentrated in classes with similar dry matter, namely classes 15 and 17%. For classes 18% and 20%, there was a representative percentage of pixels wrongly classified. It is noteworthy that class 20% exhibits a high confusion grade with class 14%.

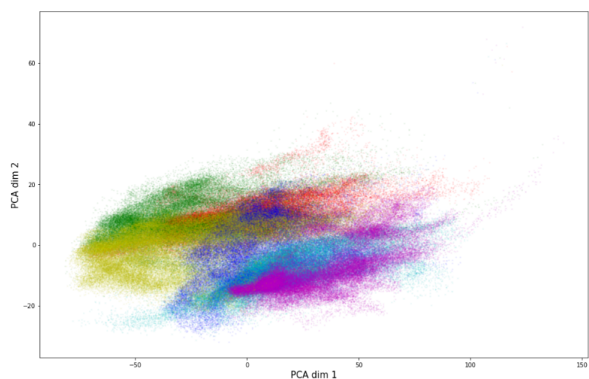
The algorithm was tested using the remaining seven avocados. Fig 5-6 represents the obtained results. The first three classes don't have any information since no more samples were available. With the results obtained in this test, it can be observed that the last avocado class has significant classification problems.

At this point, the statistic mode ([Lee and Kim, 2008]) was used to establish the corresponding class label to each test multispectral avocado image. The results can be seen in Table 5-1.

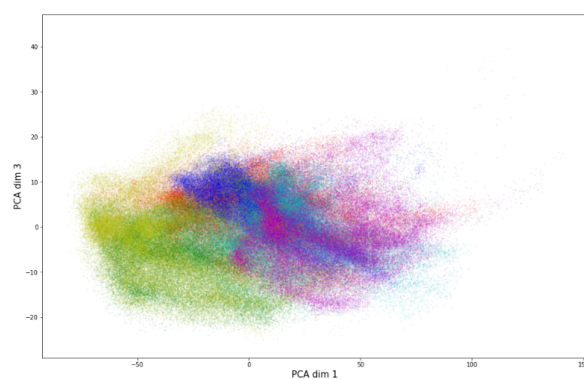
An atypical result happens with sample number six, which is an avocado that should belong to the class with label 6 (20%). However, based on the confusion matrix in Fig 5-6, it can be seen that most of the pixels are classified with the label 0 (14%).

Pixel-wise classification using the median

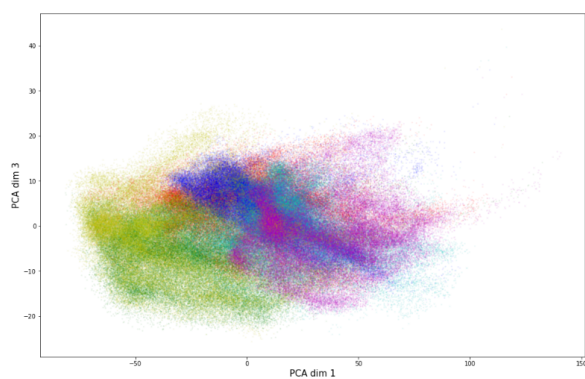
The median [Lee and Kim, 2008] is a statistic measure that represents the value at the center of the distribution, hence being unaffected by the bias that alters the mean by the presence of spurious values. In this test, each multispectral avocado image was assigned with the label corresponding to the median of the labels of each pixel inside its avocado mask, as shown in



(a) Avocados class representation PCA Dim 1 Vs Dim 2.



(b) Avocados class representation PCA Dim 1 Vs Dim 3.



(c) Avocados class representation PCA Dim 2 Vs Dim 3.

Figure 5-4.: Avocados representation after PCA reduction.

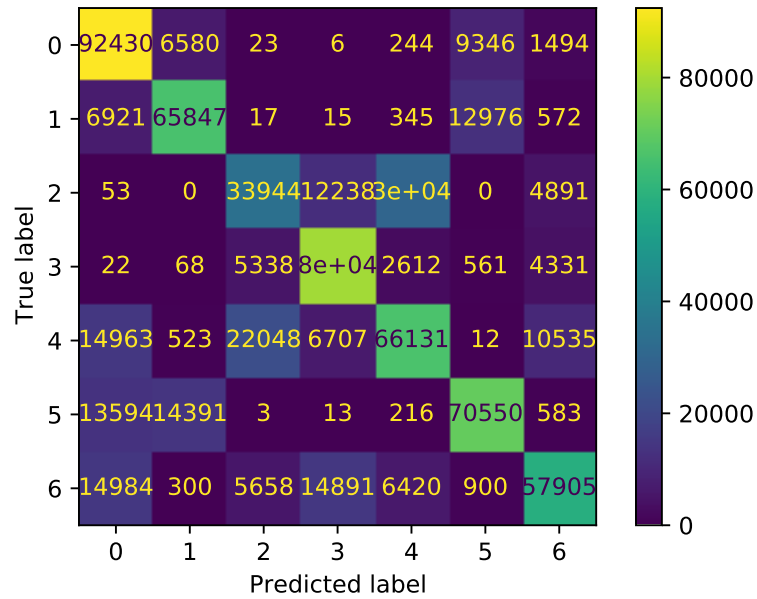


Figure 5-5.: Confusion matrix computed using the reference data.

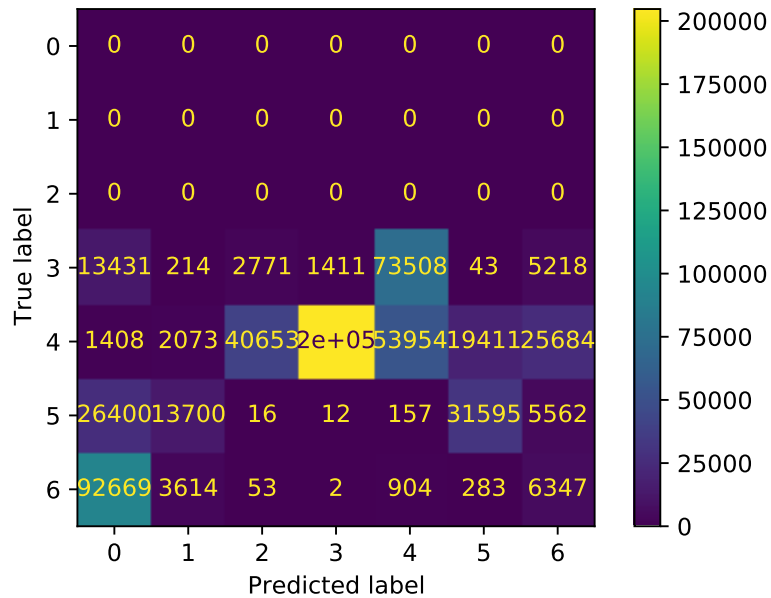


Figure 5-6.: Confusion matrix computed using remaining avocados.

Table 5-2.

In this test, the maximum error did not decrease regarding the previous tests. This can be explained by the fact that more than 50% of the pixels in sample 6 were incorrectly classified to the first class, as can be seen in Fig 5-6. Checking the other sample’s error

Table 5-1.: Avocado classification LDA with statistic mode.

Avocado	Predicted Dry matter(%)	Real Dry matter(%)	Relative Error(%)
2	19.21	18.61	3.22
6	14	19.77	29.19
8	18.27	16.93	7.91
10	17.16	18.1	5.19
11	17.16	17.64	2.72
12	17.16	17.94	4.35
14	17.16	17.77	3.43

Table 5-2.: Avocado classification LDA with statistic median.

Avocado	Predicted Dry matter(%)	Real Dry matter(%)	Relative Error(%)
2	15.59	18.61	16.23
6	14	19.77	29.19
8	18.27	16.93	7.91
10	17.16	18.1	5.19
11	18.27	17.64	3.57
12	17.16	17.94	4.35
14	17.16	17.77	3.43

percentage, it was determined that for our dataset, using the median yields a lower accuracy ([Kitchenham et al., 2001]) than using the mode.

Pixel-wise classification probabilities and statistic median value

The LDA algorithms in Scikit give us the probability of each pixel belonging to a class. The dry matter of each pixel was calculated, taking into account the probabilities. In this test, for any given pixel p , the corresponding dry matter value is computed as

$$dm_p = \sum_{i=1}^k P_i * M_i \quad (5-1)$$

where dm_p is the dry matter value of the pixel, k is the number of reference classes, $P_{p,i}$ is the probability of the pixel to belongs to the class i , and M_i is the dry matter of the class i . After getting the dry matter value of all the pixels, the median value was selected as the dry matter value of the avocado. The results obtained with this method are represented in Table 5-3

Although the error was decreased compared with the previous tests, it may still be considered as a high error. Hence, this approach was not considered a suitable method for getting the avocado dry matter with the multi-spectral images.

Table 5-3.: LDA Avocado classification with probabilities and statistic median.

Avocado	Predicted Dry matter(%)	Real Dry matter(%)	Relative Error(%)
2	16.12	18.61	13.38
6	15.6	19.77	21.09
8	18.3	16.93	8.09
10	18.74	18.1	3.54
11	18.18	17.64	3.06
12	18.87	17.94	5.18
14	19.46	17.77	9.51

5.1.2. Pixel-wise classification using the Mahalanobis distance

Mahalanobis distance ([McLachlan, 1999]) was also used to classify avocados into different classes. The reference samples were formed with the same avocados used in 5.1.1. Each class was characterized by the combination of a vector μ_i and a matrix \mathbf{S}_i , which correspond to the mean value and the covariance of the pixels contained in the class. The mean value was calculated using the EQ 5-2, and the covariance using the equation EQ 5-3. In the equations, N is the number of pixels in C_i , and $\mathbf{x}_{u,v}$ is the multispectral value of the pixel at position u, v .

$$\mu_i = \frac{1}{N} \sum_{u,v \in C_i} \mathbf{x}_{u,v} \quad (5-2)$$

$$\mathbf{S}_i = \frac{1}{N} \sum_{u,v \in C_i} (\mathbf{x}_{u,v} - \mu_i) (\mathbf{x}_{u,v} - \mu_i)^\top \quad (5-3)$$

Based on Fig 4-9, it can be assumed that in each avocado, the pixel intensity value of each wavelength tends to be concentrated. Therefore, it is possible to assume that those data points can be approximated using a b -dimensional random variable in T with a Gaussian distribution represented by $\mathcal{N}(\mu_i, \mathbf{S}_i)$ ([Peláez-García et al., 2021]).

Distance-to-class Measurement

Let U be the collection of probability distributions computed using the spectral values inside the avocado mask in the reference images. Each $U_j \in U$ is a normal distribution defined by $U_j = \mathcal{N}(\mu_j; \Sigma_j)$, related to the information in the image j . Also, let M be the collection of dry matter measurement associated to the reference images (one per image).

Now, Let C_k be the collection of spectral values of the pixels inside the avocado mask of the k -th avocado to be classified. In the collection, the spatial information of the pixels is

discarded. Then, for every element $c_{k,i} \in C_k$, let $d_{k,i,j}$ be the Mahalanobis distance from $c_{k,i}$ towards the distribution U_j . In the same sense, let $D_{k,i}$ be the collection of the Mahalanobis distances from a given sample $c_{k,i}$ of the collection C_k towards every distribution in U . Now, we choose the element $jmin$ to be the index of the minimum of the collection U ; that is,

$$jmin = \underset{j}{\operatorname{argmin}}\{U_j \in U\} \quad (5-4)$$

And we choose the element $qmin$ to be the index of the minimum of the collection $U - U_{jmin}$; that is,

$$qmin = \underset{j}{\operatorname{argmin}}\{U_j \in (U - U_{jmin})\} \quad (5-5)$$

Spectral Pixel-based Region Classification

The dry matter percentage was obtained in three different ways. The first method was to assign to each pixel the dry matter value of the class with the minimum distance as can be represented by the EQ 5-6; the square of the distance was used to avoid being affected by negative distances. After calculating the dry matter value of each pixel, the median values were obtained from all the avocados, and this was the final dry matter value assigned. In Table 5-4 are shown the results; with them can be inferred that they have even greater error than the best result obtained with LDA classification.

$$dm_p = M_{jmin} \quad (5-6)$$

Table 5-4.: Avocado classification with minimum Mahalanobis distance

Avocado	Predicted Dry matter(%)	Real Dry matter(%)	Relative Error(%)
2	19.21	18.61	3.22
6	15.59	19.77	21.14
8	18.27	16.93	7.91
10	20.34	18.1	12.38
11	20.34	17.64	15.31
12	20.34	17.94	13.38
14	20.34	17.77	14.46

The second method was to assign to each pixel a weighted value between the two minimum Mahalanobis distances, allowing the pixel to have an intermediate value between the dry

matter of the two classes. The weighted value of the dry matter for the sample $c_{k,i}$ was approximated with EQ 5-7

$$c_{k,i} = \frac{d_{k,i,jmin} * M_{qmin}}{d_{k,i,jmin} + d_{k,i,qmin}} + \frac{d_{k,i,qmin} * M_{jmin}}{d_{k,i,jmin} + d_{k,i,qmin}} \tag{5-7}$$

Table 5-5.: Avocado classification with two minimum Mahalanobis distance

Avocado	Predicted Dry matter(%)	Real Dry matter(%)	Relative Error(%)
2	17.55	18.61	5.7
6	16.85	19.77	14.77
8	19.10	16.93	12.82
10	18.93	18.1	4.59
11	18.83	17.64	6.75
12	19.03	17.94	6.08
14	19.05	17.77	7.2

As the second method improved the error, a combination of the first and second methods was implemented. The two classes with the minimum Mahalanobis distance were checked for assigning the pixel dry matter value. If the classes are consecutive (EX 17 % and 18 %) they were pondered using the same equations that in the before second method; if they were not consecutive, the dry matter value of the class with the minimum distance was taken. The results are in Table 5-6; as can be observed, no improvements were made, even the error was more significant than in the second method.

With Mahalanobis distance, the error was reduced to 14.77 %. Having better performance than the LDA methods

Table 5-6.: Avocado classification with two consecutive minimum Mahalanobis distance.

Avocado	Predicted Dry matter(%)	Real Dry matter(%)	Relative Error(%)
2	19.21	18.61	3.22
6	14.94	19.77	24.43
8	18.59	16.93	9.81
10	19.97	18.1	10.33
11	20.34	17.64	15.31
12	20.34	17.94	13.38
14	20.34	17.77	14.46

5.1.3. Self-Organizing maps classification

The self-organizing maps [TEUVO, 1990] were introduced by Teuvo Kohonen as an unsupervised Neural network. The SOM only has two layers, the input layer, and the output

layer, as explained in [KHAZRI, 2022]. The self-organizing maps have been used in several applications, notably in information representation [Richardson et al., 2003].

The self-organizing maps use a group of centroids that approximate the spatial distribution of the data in the input space, while retaining a structural relationship in the output space. In the test, a map with seven centroids organized in a one-dimensional lattice in the output space was built. The same seven avocados used in the LDA and Mahalanobis methods were selected as a references. The avocados were: 14 % = Avocado 3, 15 % = Avocado 5, 16 % = Avocado 9, 17 % = Avocado 13, 18 % = Avocado 7, 19 % = Avocado 4, 20 % = Avocado 1. Once the map is trained (as shown in Fig 5-7), each test pixel was assigned to one of the seven centroids using the euclidean distance. In this way, each point had a group of pixels that belonged to it. Then, a dry matter value was assigned to each centroid based on the pixels in their respective group. The value of the dry matter was evaluated by the mean and the median of the group. The results are consigned in Table 5-7. As it happened with the mean, all the values are close to 17%, which means that the extreme values are not being properly represented using the mean value. Therefore, the median was chosen instead.

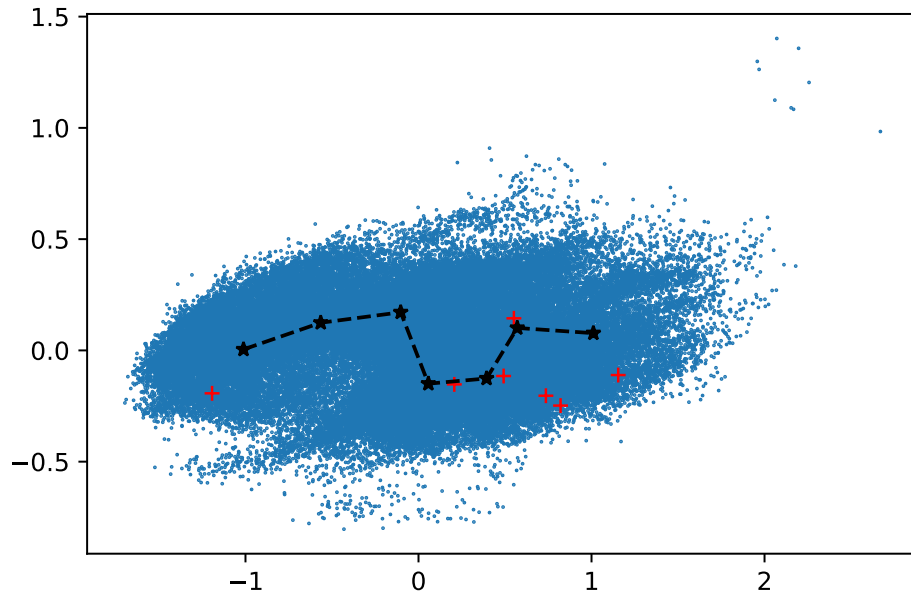


Figure 5-7.: Self-organized maps with 7 avocados and 7 points

Table 5-7.: Self-organized points gotten values by mean.

Measure	P1(dm)	P2(dm)	P3(dm)	P4(dm)	P5(dm)	P6(dm)	P7(dm)
mean	17.49	16.28	16.79	18.14	17.62	16.92	17.10
median	19.21	15.59	15.59	18.27	17.16	16.27	17.16

The values of the dry matter of the pixels in the test multispectral avocado images were calculated using the map. The dry matter of each pixel was assigned according to the dry matter of the closest centroid in the map; and the avocado dry matter results from the median of the dry matter associated to the pixels inside the avocado mask in the image. A summary of the results is presented in Table 5-8. From the results, we can see that the error generally decreased, but the maximum error was significant compared with the lowest error obtained using the Mahalanobis distance.

Table 5-8.: Avocado classification with 7 avocados using self-organized maps.

Avocado	Predicted Dry matter(%)	Real Dry matter(%)	Relative Error(%)
2	19.21	18.61	3.22
6	16.27	19.77	17.7
8	17.16	16.93	1.36
10	17.16	18.1	5.19
11	18.27	17.64	3.57
12	17.16	17.94	4.35
14	17.16	17.77	3.43

Overall, in our tests, the best dry matter estimation was achieved using Mahalanobis distance, while the worst was achieved with LDA. It is noteworthy that, even though we had lots of pixels to build the models, there is significant uncertainty due to the low number of reference and test specimens (avocados).

6. Conclusions and future work

6.1. Conclusions

One of the main objectives of the enclosure was to isolate the captured images from the influence of external lights. To verify the attainment of this requirement, some tests were performed under different external light conditions with the internal LEDs off, achieving less than 5% in the intensity of the acquired images. Therefore, we can conclude that the system's external light influence was successfully minimized. Additionally, the reflective properties of the internal surfaces of the structure were tested by turning on three power LEDs (3W approx.) with an incident angle of 45 degrees between the light source and the camera. The intensity in the images were less than 10%, which means that the MDF surface painted with black 3.0 has enough absorption to avoid undesired internal reflection. Finally, it is worth mentioning that the parameters used for the image acquisition in this test were the same used with the avocados image captures.

The hardware design for controlling the LED-base multispectral light was verified by measuring the nominal current for each of the eight different groups of LEDs. In addition, the brightness level is determined by a PWM signal generated by the MCU and used as input on the IC LED controller. The robustness and correct functioning of the IC LED controller allows us to discard the option of controlling the LED nominal current with a series resistor.

A mechanism to change the angle of the light source was implemented to control the specular and diffused light. After testing with different angles, no collisions were detected between the light and the structure.

The major challenge in firmware development was defining the appropriate interface to synchronize the lights from different boards. The firmware architecture was designed to optimize the answer time of the synchronization tasks by releasing the CPU from performing tasks that specialized peripherals, such as timers for PWM generation signals, can do. The UART interface communication was tested with one-meter cables at 115200 bauds. The communication latency was tested with four boards on the system. Four GPIOs helps to maintain the boards synchronized, minimizing the effects of the latency generated by the communication. The ID protocol based on master-slave configuration achieves effective communication between all the boards. In addition, the protocol includes a series of commands which allow controlling the hardware.

A demonstration of the LED-based imaging system functioning was performed with both; a color-checker and avocados in different ripening states. The color-checker captures show how the color changes depending on the wavelength used. In addition, the histograms of the avocados provide discriminant information between different ripening states.

As mentioned in [Lee et al., 1983], there is a relation between the dry matter and the ripening state of the avocado. Therefore an association between the dry matter and the multispectral captures was investigated. The dry matter extraction was done based on [Carvalho et al., 2015]. Two samples were taken per avocado to confirm the method's accuracy. The wavelengths used in the captures were: 451nm, 500nm, 525nm, 550nm, 620nm, 660nm, 740, and 850 nm. The tested algorithms were LDA, Mahalanobis distances, and Self-organized maps; the method with better performance was the Mahalanobis distance which had a maximum relative error of 14.77 %

6.2. Future work

In the future, the system can be used to find different characteristics in different agricultural products like coffee beans, citrus fruits, and others. For this purpose, the system was constructed to test different wavelengths, like far infrared. The captures in this thesis were taken with the flea camera; it is possible to check the information gotten with other cameras like a Nikon camera or a SWIR camera which has better performance in wavelengths larger than 800nm. Having an API for the use of the system would help for an easier configuration and captures with the system.

Characterizing the LEDs will be essential to understand the behavior of the LEDs inside the structure; it was not done in this thesis, but in the future, it will help to reduce the shadows and the specular light present in the images.

Duty the time was not possible to take many samples; it would be essential to take more samples and test the before described algorithm. Also, Advanced Neural network techniques can be implemented to compare with the current classification techniques.

A. Anexo: Total variation in specular light

The specular light is a common problem in image capturing; if it is not checked adequately, it can generate high saturation on the capture. The amount of specular light present in an image is directly related to the angle between the light source and the camera; with a 0° angle, there will be a high amount of specular light, and with a 90° angle, it is the minimum. On the other side is the diffuse light; this one will give the relevant information about the object; the diffuse light also depends on the angle between the camera and the light source; having its maximum amount at 0° and its minimum amount a 90° .

Total variation is a method that calculates the variability in the pixel intensity of an image; a high degree of variability in the image would mean a high presence of specular light, while a low amount of variation would imply a high amount of diffuse light.

In this study, we tried to find the best angle between the camera and a light source, aspiring to obtain the highest possible illumination and the least amount of specular light present (low total variation). For this purpose, we will explain the procedure used to take the images, the algorithms used to analyze the data obtained, and the results obtained. In Fig **A-1**, there is a block diagram of the workflow.

A.0.1. Tools

The system used a multispectral light bar, which has a total of 24 LEDs belonging to eight different waves (3 LEDs per wave); each light was able to be graduated its intensity level from 10 to 100%, as shown in Fig **A-2**. In addition, the system has a microcontroller capable of changing the brightness level of the LEDs, which is in charge of checking the system status and triggering the image capture at the right time. The actual controller can be seen in Fig **A-3**. Captures were made with a flea3 FL3-GE-03S1M-C multispectral camera.

A.0.2. Setup

A 20 x 20 cm white acrylic was used; this acrylic has a matte vinyl to decrease the amount of specular light produced by a glossy surface, trying to achieve a Lambertian surface. Fig **A-4**. The camera and the light source shall be at a distance of 30 cm from the lens.

In the experiment, six different angles were tested between the camera and the light board;

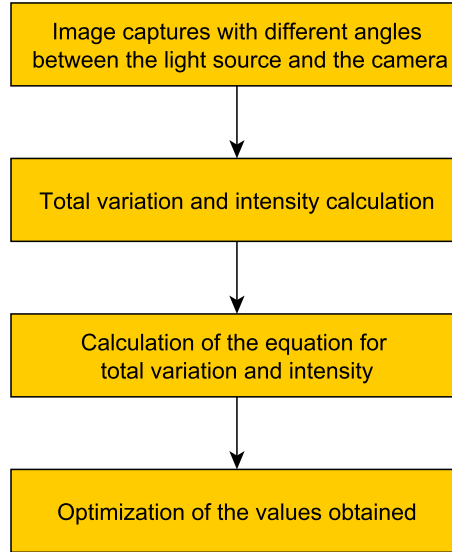


Figure A-1.: Total variation in specular light HLBD.

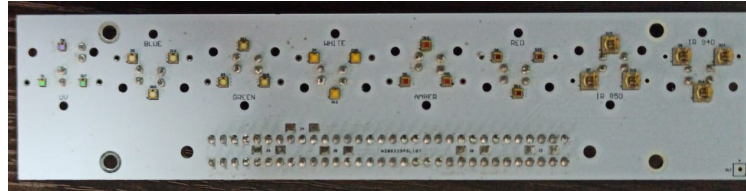


Figure A-2.: LEDs bar.

ten images were taken and averaged for noise reduction effects for each angle. 3 LEDs were used on the light board with a PWM of 50%. The angles used were 0° , 15° , 30° , 45° , 60° , 75° . The reflectance maps obtained from the averaged images can be seen in Fig A-5

A.0.3. Total variation

Through the total variation presented in the images, we can observe an alternate way of calculating the scattered light in the image. based on [Flamary, 2022] have been obtained the equation EQ A-1. Where x_i are the pixels of the image, and x_j are the four neighboring pixels of x_i . Based on this formula and the python programming language, we were able to obtain the total variation in all the images, which is represented in Table A-1

$$TV = \sum_{i,j \in N} \| \mathbf{x}_i - \mathbf{x}_j \|_2^2 \quad (\text{A-1})$$

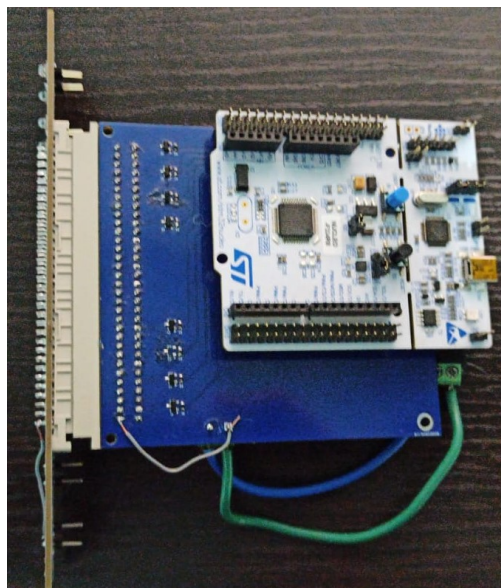


Figure A-3.: Control board.



Figure A-4.: Setup

A.0.4. Total intensity

The total intensity of the image was calculated in Python based on the equation A-2 where x_i refers to the intensity value obtained by the camera. The total intensity values are shown in Table A-2

$$TI = \sum_{i \in N} x_i \quad (\text{A-2})$$

A.0.5. Equation approximation using algorithms

In Python, algorithms were developed to find two equations of the form $Ax^2 + bx + c$. The first represents the change in total intensity as a function of angle, and the second represents the change in total variation as a function of angle. For ease of visualization and programming,

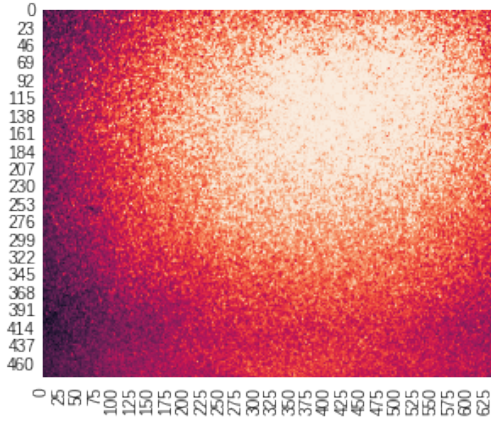
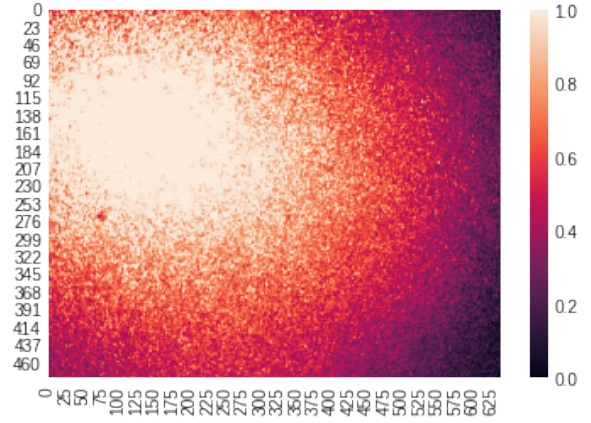
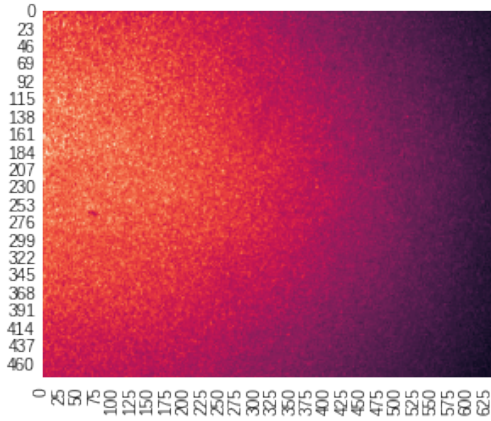
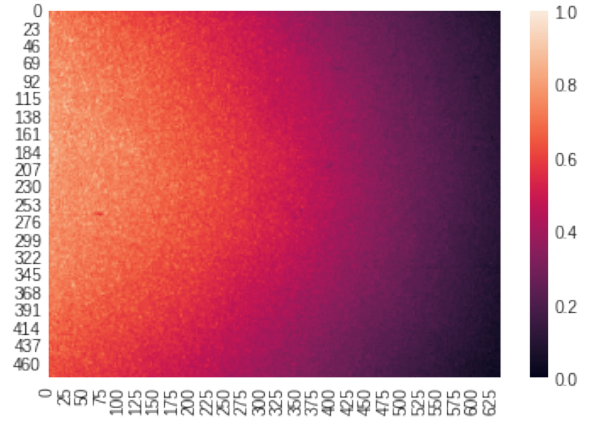
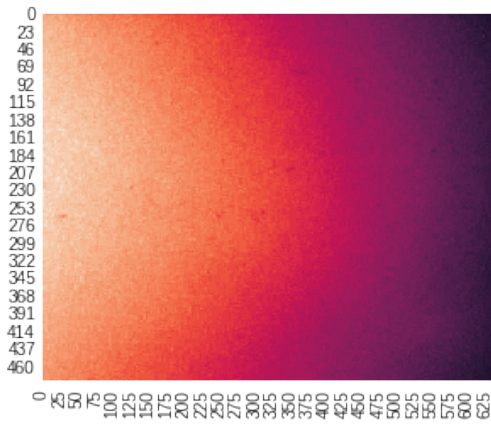
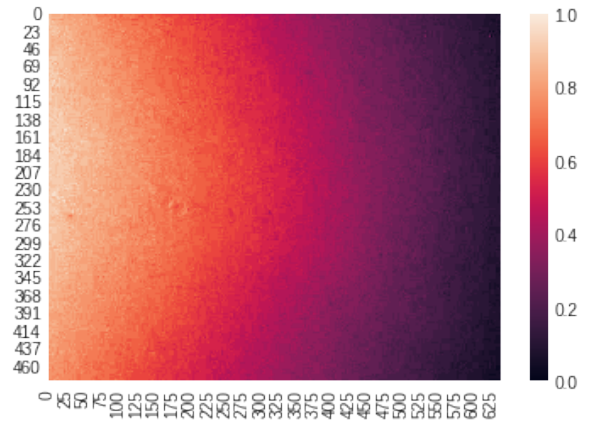
(a) Heat map with angle 0° .(b) Heat map with angle 15° .(c) Heat map with angle 30° .(d) Heat map with angle 45° .(e) Heat map with angle 60° .(f) Heat map with angle 75° .**Figure A-5.:** Captured heat maps.

Table A-1.: Total variation vs angle.

Ángle	Total variation
0	2701583
15	2007127
30	1573302
45	844367
60	443712
75	291422

Table A-2.: Total intensity vs angle.

Ángle	Total intensity
0	72796976
15	72933329
30	64160269
45	56991544
60	44709958
75	24921573

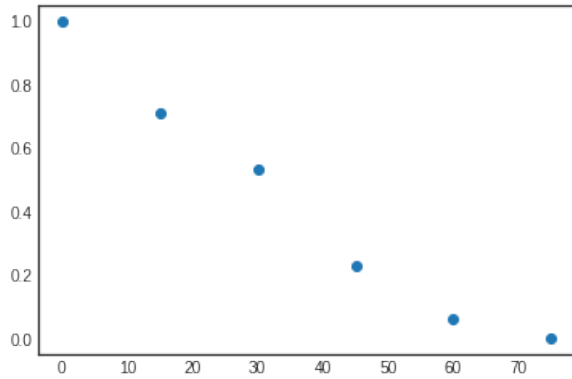
the total variation data were normalized with the equation: $(x_i - \text{mín}(x)) / (\text{máx}(x) - \text{mín}(x))$. The data remained at its values between 0 and 1; the normalized values of total variation and intensity in the different images as a function of the angle are shown in fig **A-6**.

Using a least squares error minimization, the values of A, B, and C of the equation: $Ax^2 + bx + c$ were found. The values obtained for the total variation were: A = 0.0000936, B = -0.02082, and C = 1.010697, and for the total intensity, were: A = -0.0001878, B = 0.0009507, and C = 1. The graphs obtained from the equations vs. the real measured points are represented in fig **A-7**. In fig **A-6b** it is observed that the graph resembles a cosine function, which is congruent with the equation A-3 found in the book [Jain et al., 1995], in which L refers to the total radiation, and θ_s refers to the angle between the light has and the camera.

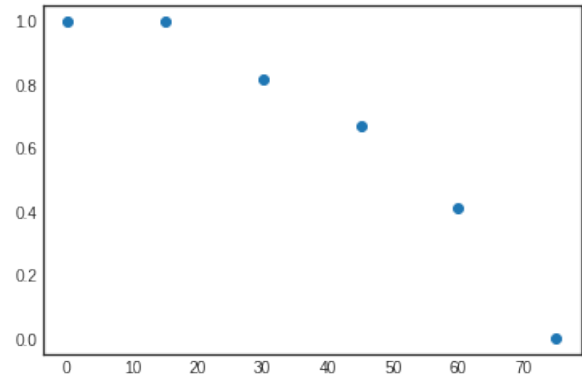
$$L(\theta_c, \phi_c) = I_0 / \pi * \cos(\theta_s) \tag{A-3}$$

A.0.6. Optimization

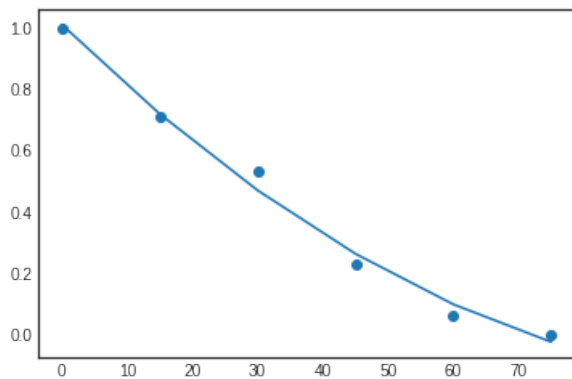
Starting from the equations obtained in the previous subsection can proceed to perform a multiobjective optimization; the new cost function will be $Cost = \alpha * TV - (1 - \alpha) * TI$, where α will have a value between 0 and 1 and which will indicate which of the two objectives will have greater importance. In this case, have been selected a value of $\alpha 0.4$; with this value, more importance is given to having a high intensity, sacrificing a little the total variation. The graph of the new cost function can be seen in Fig [refFig:function cost](#). Graphically and mathematically, it can be seen that the optimal angle with a $\alpha = 0,4$ will be 30° .



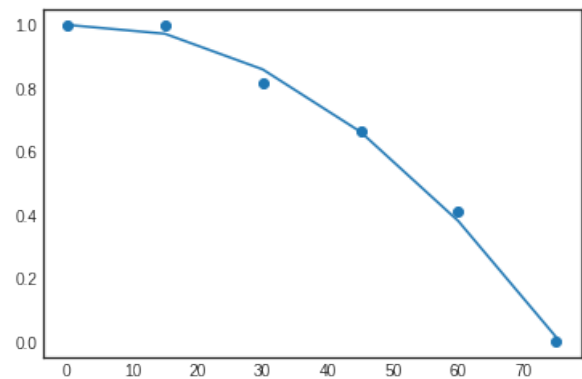
(a) Total variation vs angle.



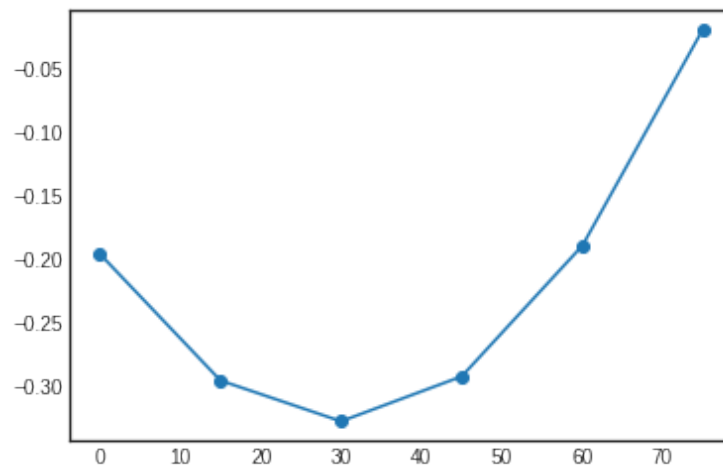
(b) Total intensity vs angle.

Figure A-6.: Obtained graphs.

(a) Equation total variation as a function of angle.



(b) Equation total intensity as a function of angle.

Figure A-7.: Equation graphs obtained.**Figure A-8.:** Cost function graph.

Bibliografía

- [LED, 2022a] (2022a). Luxeon cz color line maximum punch in any application. https://www.mouser.com/datasheet/2/602/DS198_luxeon_cz_color_line_datasheet-2950619.pdf. Accessed: 2022-12-20.
- [LED, 2022b] (2022b). Sfh 4714a. <https://www.mouser.com/ProductDetail/ams-OSRAM/SFH-4714A?qS=xC%252BE9h5iuX7Z4m%2FWjFDmxg%3D%3D>. Accessed: 2022-12.
- [LED, 2022c] (2022c). Xlamp® xp-e2 leds. <https://www.mouser.com/datasheet/2/723/XLampXPE2-2327163.pdf>. Accessed: 2022-12.
- [Adams et al., 2019] Adams, A., Nicol, F., McHugh, S., Moore, J., Matis, G., and Amparan, G. A. (2019). Vantablack properties in commercial thermal infrared imaging systems. In *Infrared Imaging Systems: Design, Analysis, Modeling, and Testing XXX*, volume 11001, pages 329–339. SPIE.
- [Albin et al., 2002] Albin, S., Rougeron, G., Péroche, B., and Trémeau, A. (2002). Quality image metrics for synthetic images based on perceptual color differences. *IEEE transactions on image processing*, 11(9):961–971.
- [Ataer-Cansizoglu et al., 2015] Ataer-Cansizoglu, E., Bolon-Canedo, V., Campbell, J. P., Bozkurt, A., Erdogmus, D., Kalpathy-Cramer, J., Patel, S., Jonas, K., Chan, R. P., Ostmo, S., et al. (2015). Computer-based image analysis for plus disease diagnosis in retinopathy of prematurity: performance of the “i-rop” system and image features associated with expert diagnosis. *Translational vision science & technology*, 4(6):5–5.
- [Atkins et al., 2001] Atkins, C. B., Bouman, C. A., and Allebach, J. P. (2001). Optimal image scaling using pixel classification. In *Proceedings 2001 International Conference on Image Processing (Cat. No. 01CH37205)*, volume 3, pages 864–867. IEEE.
- [Avila, 2022] Avila, J. (2022). Linear discriminant analysis. https://www.jacobsoft.com.mx/es_mx/linear-discriminant-analysis/. Accessed: 2022-12.
- [Bustard and Nixon, 2010] Bustard, J. D. and Nixon, M. S. (2010). Toward unconstrained ear recognition from two-dimensional images. *IEEE transactions on systems, man, and cybernetics-Part A: Systems and Humans*, 40(3):486–494.

- [Carvalho et al., 2015] Carvalho, C., Velásquez, M., and Van Rooyen, Z. (2015). Porcentaje mínimo de materia seca para una cosecha adecuada del aguacate cv.‘hass’ en colombia. In *VIII World Avocado Congress*, pages 13–18.
- [Choubey et al., 2020] Choubey, D. K., Kumar, M., Shukla, V., Tripathi, S., and Dhandhanina, V. K. (2020). Comparative analysis of classification methods with pca and lda for diabetes. *Current diabetes reviews*, 16(8):833–850.
- [CULTUREHUSTLE, 2023] CULTUREHUSTLE (2023). You’re looking at the world’s blackest black point. <https://culturehustle.com/products/black-3-0-the-worlds-blackest-black-acrylic-paint-150ml>. Accessed: 2023-01.
- [Doshi et al., 2013] Doshi, J., Erus, G., Ou, Y., Gaonkar, B., and Davatzikos, C. (2013). Multi-atlas skull-stripping. *Academic radiology*, 20(12):1566–1576.
- [Eden et al., 2006] Eden, A., Uyttendaele, M., and Szeliski, R. (2006). Seamless image stitching of scenes with large motions and exposure differences. In *2006 IEEE Computer Society Conference on Computer Vision and Pattern Recognition (CVPR’06)*, volume 2, pages 2498–2505. IEEE.
- [Ejury, 2013] Ejury, J. (2013). Buck converter design. *Infineon Technologies North America (TFNA) Corn Desion Note*, 1:1.
- [ETC, 2022] ETC (2022). Mg995 high speed metal gear dual ball bearing servo. <https://datasheetspdf.com/pdf-file/839879/ETC/MG995/1>. Accessed: 2022-12.
- [Flamary, 2022] Flamary, R. (2022). Total variation in images. Accessed: 2022-12.
- [Grey, 2022] Grey, P. (2022). Flea3 gige gige digital camera technical reference. <https://flir.app.boxcn.net/s/9wswc4xcu9u0wsq7v6o54c84exjvrn00>. Accessed: 2022-12.
- [Grey, 2023] Grey, P. (2023). Getting started with theflea3 gige digital camera. https://robosub.eecs.wsu.edu/wiki/_media/cs/cameras/fl3-ge_gettingstarted.pdf. Accessed: 2023-01.
- [Gupta, 2019] Gupta, A. (2019). Uart communication. In *The IoT Hacker’s Handbook*, pages 59–80. Springer.
- [Jain et al., 1995] Jain, R., Rangachar, K., and Brian, G. (1995). *Machine vision*.
- [John, 2022] John (2022). Spi vs. uart: Serial communication protocols for micro-controllers and embedded systems. <https://www.digikey.com/en/articles/uarts-ensure-reliable-long-haul-industrial-communications#:~:text=With%20appropriate%20line%20drivers%2C%20a,485%20or%20RS%2D422%20interfaces>. Accessed: 2022-12.

- [KEYENCE, 2023] KEYENCE (2023). Vision system peripheral equipment. <https://www.keyence.com/mykeyence/?ptn=001>. Accessed: 2023-01.
- [KHAZRI, 2022] KHAZRI, A. (2022). Self organizing maps. <https://towardsdatascience.com/self-organizing-maps-1b7d2a84e065>. Accessed: 2019-08-7.
- [Kim et al., 2007] Kim, H., Drake, B. L., and Park, H. (2007). Multiclass classifiers based on dimension reduction with generalized lda. *Pattern Recognition*, 40(11):2939–2945.
- [Kim et al., 2004] Kim, M. S., Lefcourt, A. M., and Chen, Y.-R. (2004). Multispectral fluorescence imaging techniques for nondestructive food safety inspection. In *Monitoring Food Safety, Agriculture, and Plant Health*, volume 5271, pages 62–72. SPIE.
- [Kitchenham et al., 2001] Kitchenham, B. A., Pickard, L. M., MacDonell, S. G., and Sheperd, M. J. (2001). What accuracy statistics really measure. *IEE Proceedings-Software*, 148(3):81–85.
- [LEDnique, 2022] LEDnique (2022). Simple constant-current driver. <http://lednique.com/power-supplies/simple-constant-current-driver/>. Accessed: 2022-11.
- [Lee et al., 1983] Lee, S., Young, R., Schiffman, P., and Coggins, C. (1983). Maturity studies of avocado fruit based on picking dates and dry weight. *J. Amer. Soc. Hort. Sci.*, 108(3):390–394.
- [Lee and Kim, 2008] Lee, Y.-G. and Kim, S.-Y. (2008). Introduction to statistics. *Yulgok-books, Korea*, pages 342–351.
- [Liu et al., 2022] Liu, X., Tian, Y., Chen, F., Ahlgren, R., Zheng, Y., Su, M., Xiao, G., and Zheng, Y. (2022). An efficient and scalable strategy for ultrablack-paint-enabled solar-driven steam generation. *Solar Energy Materials and Solar Cells*, 234:111436.
- [Lyu, 2019] Lyu, Y. (2019). *Identify the ripening stage of avocado by multispectral camera using semi-supervised learning on small dataset*. PhD thesis.
- [Martin, 2009] Martin, D. (2009). A practical guide to machine vision lighting. advanced illumination.
- [Matusik, 2003] Matusik, W. (2003). A data driven reflectance model.
- [McLachlan, 1999] McLachlan, G. J. (1999). Mahalanobis distance. *Resonance*, 4(6):20–26.
- [Moscibroda and Wattenhofer, 2006] Moscibroda, T. and Wattenhofer, R. (2006). The complexity of connectivity in wireless networks. In *INFOCOM 2006: 25th Annual Joint Conference of the IEEE Computer and Communications Societies, Barcelona, Spain*.

- [Myint et al., 2011] Myint, S. W., Gober, P., Brazel, A., Grossman-Clarke, S., and Weng, Q. (2011). Per-pixel vs. object-based classification of urban land cover extraction using high spatial resolution imagery. *Remote sensing of environment*, 115(5):1145–1161.
- [Narra and Zinger, 2004] Narra, P. and Zinger, D. S. (2004). An effective led dimming approach. In *Conference Record of the 2004 IEEE Industry Applications Conference, 2004. 39th IAS Annual Meeting.*, volume 3, pages 1671–1676. IEEE.
- [Naseer et al., 2016] Naseer, N., Noori, F. M., Qureshi, N. K., and Hong, K.-S. (2016). Determining optimal feature-combination for lda classification of functional near-infrared spectroscopy signals in brain-computer interface application. *Frontiers in human neuroscience*, 10:237.
- [Onsemi, 2022] Onsemi (2022). High-side sensing constant current buck controller for high switching frequency led driver fl7760. <https://www.onsemi.com/pdf/datasheet/fl7760-d.pdf>. Accessed: 2022-12.
- [Ordoñez, 2019] Ordoñez, C. E. A. (2019). Protocolo para la determinación de materia seca de frutos de aguacate (persea americana mill. cv. hass) con horno microondas.
- [Peinado et al., 2020] Peinado, V. P., Cadavid, D. F. N., et al. (2020). Potencial exportador de aguacate colombiano a corea del sur. *Online Journal Mundo Asia Pacifico*, 9(17):90–103.
- [Peláez-García et al., 2021] Peláez-García, C., Patiño-Martínez, V.-A., Gómez-Mendoza, J.-B., and Tamayo-Monsalve, M.-A. (2021). A framework for multispectral instance classification using examples. In *Workshop on Engineering Applications*, pages 493–504. Springer.
- [Pini, 2023] Pini, A. (2023). Uarts ensure reliable long-haul industrial communications over rs-232, rs-422, and rs-485 interfaces. <https://www.ourpcb.com/spi-vs-uart.html>. Accessed: 2023-01.
- [Qin et al., 2009] Qin, J., Burks, T. F., Ritenour, M. A., and Bonn, W. G. (2009). Detection of citrus canker using hyperspectral reflectance imaging with spectral information divergence. *Journal of food engineering*, 93(2):183–191.
- [REY, 2022] REY, A. D. (2022). Fuit specifications. <https://www.delreyavocado.com/growers/fruit-specifications/>. Accessed: 2022-12.
- [Richardson et al., 2003] Richardson, A. J., Risien, C., and Shillington, F. A. (2003). Using self-organizing maps to identify patterns in satellite imagery. *Progress in Oceanography*, 59(2-3):223–239.
- [Ringnér, 2008] Ringnér, M. (2008). What is principal component analysis? *Nature biotechnology*, 26(3):303–304.

- [Room, 2019] Room, C. (2019). Confusion matrix. *Mach. Learn*, 6:27.
- [Sampat et al., 2002] Sampat, M. P., Castleman, K., and Bovik, A. (2002). Pixel-by-pixel classification of mfish images. In *Proceedings of the Second Joint 24th Annual Conference and the Annual Fall Meeting of the Biomedical Engineering Society*[[*Engineering in Medicine and Biology*, volume 2, pages 999–1000. IEEE.
- [scikit learn, 2022] scikit learn (2022). sklearn.decomposition.pca. <https://scikit-learn.org/stable/modules/generated/sklearn.decomposition.PCA.html>. Accessed: 2022-11.
- [SEMICONDUCTOR, 2022] SEMICONDUCTOR, T. (2022). Tsm2302cx. <https://www.onsemi.com/pdf/datasheet/f17760-d.pdf>. Accessed: 2022-12.
- [Sharma et al., 2006] Sharma, A., Paliwal, K. K., and Onwubolu, G. C. (2006). Class-dependent pca, mdc and lda: a combined classifier for pattern classification. *Pattern Recognition*, 39(7):1215–1229.
- [Speer et al., 2008] Speer, R., Havasi, C., and Lieberman, H. (2008). Analogyspace: Reducing the dimensionality of common sense knowledge. In *Aaai*, volume 8, pages 548–553.
- [ST, 2021] ST (2021). Technical bulletin stmicroelectronics’ 17983 and 16983 synchronous step-down converters. https://www.st.com/resource/en/technical_article/st_coilcraft_17983_16983-stcoilcraft-17983-16983-stmicroelectronics.pdf. Accessed: 2022-12.
- [Sun et al., 2000] Sun, M.-T., Feng, W.-C., Lai, T.-H., Yamada, K., Okada, H., and Fujimura, K. (2000). Gps-based message broadcast for adaptive inter-vehicle communications. In *Vehicular technology conference fall 2000. IEEE VTS fall VTC2000. 52nd vehicular technology conference (Cat. No. 00CH37152)*, volume 6, pages 2685–2692. IEEE.
- [Tamayo Monsalve, 2020] Tamayo Monsalve, M. A. (2020). Diseño de un sistema de adquisición de imágenes multiespectrales basado en iluminación led de potencia de ancho de banda estrecho.
- [TEUVO, 1990] TEUVO, K. (1990). The self-organizing map. 78:482–488.
- [Zhang et al., 2015] Zhang, L., Zhang, Q., and Xiao, C. (2015). Shadow remover: Image shadow removal based on illumination recovering optimization. *IEEE Transactions on Image Processing*, 24(11):4623–4636.